J Therm Spray Tech (2018) 27:603–623
https://doi.org/10.1007/s11666-018-0702-6

PEER REVIEWED

Cold Spray Aluminum–Alumina Cermet Coatings: Effect of Alumina Content

Ruben Fernandez[1] · **Bertrand Jodoin**[2]

Submitted: 3 February 2017 / in revised form: 24 January 2018 / Published online: 8 February 2018

Abstract Deposition behavior and deposition efficiency were investigated for several aluminum–alumina mixture compositions sprayed by cold spray. An increase in deposition efficiency was observed. Three theories postulated in the literature, explaining this increase in deposition efficiency, were investigated and assessed. Through finite element analysis, the interaction between a ceramic particle peening an impacting aluminum particle was found to be a possible mechanism to increase the deposition efficiency of the aluminum particle, but a probability analysis demonstrated that this peening event is too unlikely to contribute to the increment in deposition efficiency observed. The presence of asperities at the substrate and deposited layers was confirmed by a single-layer deposition efficiency measurement and proved to be a major mechanism in the increment of deposition efficiency of the studied mixtures. Finally, oxide removal produced by the impact of ceramic particles on substrate and deposited layers was evaluated as the complement of the other effects and found to also play a major role in increasing the deposition efficiency. It was found that the coatings retained approximately half of the feedstock powder alumina content. Hardness tests have shown a steady increase with the coating alumina content. Dry wear tests have revealed no improvement in wear resistance in samples with an alumina content lower than 22 wt.% compared to pure aluminum coatings. Adhesion strength showed a steady improvement with increasing alumina content in the feedstock powder from 18.5 MPa for pure aluminum coatings to values above 70 MPa for the ones sprayed with the highest feedstock powder alumina content.

Keywords aluminum–alumina · cermet · cold spray · deposition efficiency

✉ Ruben Fernandez
rufernan@ing.uchile.cl

[1] Faculty of Physical and Mathematical Science, University of Chile, Santiago, Chile

[2] Cold Spray Research Laboratory, University of Ottawa, Ottawa, ON, Canada

Introduction

Ceramic–metal composites, most commonly known as cermets, are composites materials made of ceramics and metals. Cermets are designed to retain the optimal properties of its components, such as ductility and toughness of metals, along with the hardness and wear resistance of ceramics (Ref 1-4). Typical production methods used to consolidate cermets include compaction and sintering, hot extrusion, and infiltration (Ref 2, 4). Thermal spray processes have also been used for the production of cermet materials by spray deposition. A recent proposed alternative is the deposition by cold gas dynamic spraying, more often referred to as cold spray. The cold spray process accelerates feedstock powders (usually metals) using a supersonic gas stream generated by a De Laval-type nozzle (Ref 5-7). Due to the relatively low gas temperatures resulting from the rapid gas expansion in the nozzle, the feedstock powders remain solid throughout their flight (Ref 8-10). When the particles impact the substrate, they experience extensive plastic deformation (Ref 8, 11). These particles adhere to the substrate either by mechanical anchoring or, if enough plastic deformation is obtained, by metallurgical bonding (Ref 5, 8, 12-15). To cold spray cermets, reinforcement particles are mixed with ductile

metallic feedstock powders. During deposition, a fraction of the reinforcement particles is retained into the final coating (Ref 16-19). Hard reinforcement particles do not experience severe plastic deformation such as the ones observed in the ductile materials, but rather induce more plastic deformation of the ductile phase (Ref 16, 17). These particles adhere to the coating, normally by embedding themselves in the coating producing the cermet (Ref 19, 20).

Several ceramic–metal combinations have been successfully deposited by cold spray with a variety of powder morphologies (Ref 16, 17, 21-36). The applications and sought coating properties closely resemble the ones seen in other thermal spray processes, principally wear resistance, high hardness, and high-temperature applications. The inclusion of ceramic particles is the main cause of improvement of these properties when compared with the ductile metallic phase. The addition of ceramic particles does not just affect the coating properties but also has a substantial effect on the deposition process behavior. Even though the deposition of ceramic–metal mixtures has been extensively studied in cold spray and the properties and deposition behavior have been established, most of these studies have been exploratory and have used a descriptive approach with a focus on industrial applications (Ref 18, 34-39). A few studies have been performed with the purpose of explaining the behavior observed, and a few theories have been proposed to account for the effect of ceramic particles in the feedstock powder (Ref 16, 17, 19, 28, 37, 40-42).

One of the most dramatic changes in deposition behavior observed with the addition of ceramic particles to ductile feedstock powder is the increase in deposition efficiency (DE). This behavior was first reported in a study where mixtures of Al-Al_2O_3 at different weight ratios were deposited (Ref 19). They noticed an increase in DE with the addition of Al_2O_3 particles with a peak at 30 wt.% Al_2O_3 and a decrease in DE at higher feedstock powder ceramic contents, eventually reaching 0% DE at 95 wt.% ceramic. Several other investigations have shown similar trends in deposition efficiency (Ref 16, 28, 40).

This increase in DE was not initially expected, as the cold spray of ceramics only leads to substrate erosion (Ref 43, 44). Another study used the coating ceramic content to compute the partial deposition efficiency of both the metallic and ceramic particles (Ref 16). This showed that the DE increase could not be solely attributed to ceramic particles embedding into the coating, but rather to an interaction between the ceramic and the metallic powder particles, with the DE of the aluminum particles increasing with the addition of ceramic particles into the feedstock powder (Ref 16). Consequently, aluminum particles have an increased probability to adhere to the substrate when they are in the presence of ceramic particles. This increase in partial DE of aluminum is observed up to high wt.% of ceramic in the feedstock powder. Therefore, the decrease in the overall DE at higher wt.% of ceramic is the result of the low DE of ceramic particles, and its influence gets more relevant as its weight contribution in the feedstock powder increases.

Investigations have provided some explanations for the observed DE increase with the addition of ceramic particles into the feedstock powder. The peening or impingement effect was described in one study, in which they sprayed different metals and ceramics (Ref 42). They proposed that a hard ceramic particle acts as shot balls, peening the soft particles in front of it, increasing its deformation, and as a consequence, increasing the softer metallic particles deposition efficiency. This proposed mechanism has been mentioned in other investigations but has never been verified (Ref 18, 40).

Another mechanism was proposed in two separate studies (Ref 16, 19). In their investigations, it was observed that the interface between the coating and substrate roughens as the percentage of ceramic in the feedstock mixture increases. This increase in roughness is expected due to the grit blasting effect of the impacting alumina particles onto the substrate. At a higher ceramic percentage in the mixture, more alumina particles blast the substrate/coating. It was suggested that these asperities are helping bonding more particles, increasing the deposition efficiency of the mixture due to a higher probability of obtaining mechanical anchoring (Ref 16). This potential mechanism has been used as an explanation in other investigations as a possible mechanism but has never been verified (Ref 17, 21).

Finally, the last potential mechanism suggested in the literature is referred to as the oxide cleaning effect of ceramic particles impacting the metallic particles/substrate. This explanation describes the ceramic particles deforming and removing the native oxide film of the metallic particles/substrate upon impact, exposing new fresh metal surfaces and leaving them ready for the impact of the next metallic particle for the creation of a favorable metallurgical bonding site. This effect might also be achieved by pure deformation, as the oxide layer is brittle and may crack leaving oxide-free locations that could lead to the increase of DE observed (Ref 45). This effect has been described before in cold spray, but it has not been proved to be the responsible in increasing the DE (Ref 9, 28, 46, 47). These three mechanisms potentially explaining the increase in DE are illustrated in Fig. 1.

Another important point to take into account when ceramic particles are added to the feedstock powder is that erosion might occur to the substrate/metallic particles. Erosion by solid particles has been extensively studied (Ref

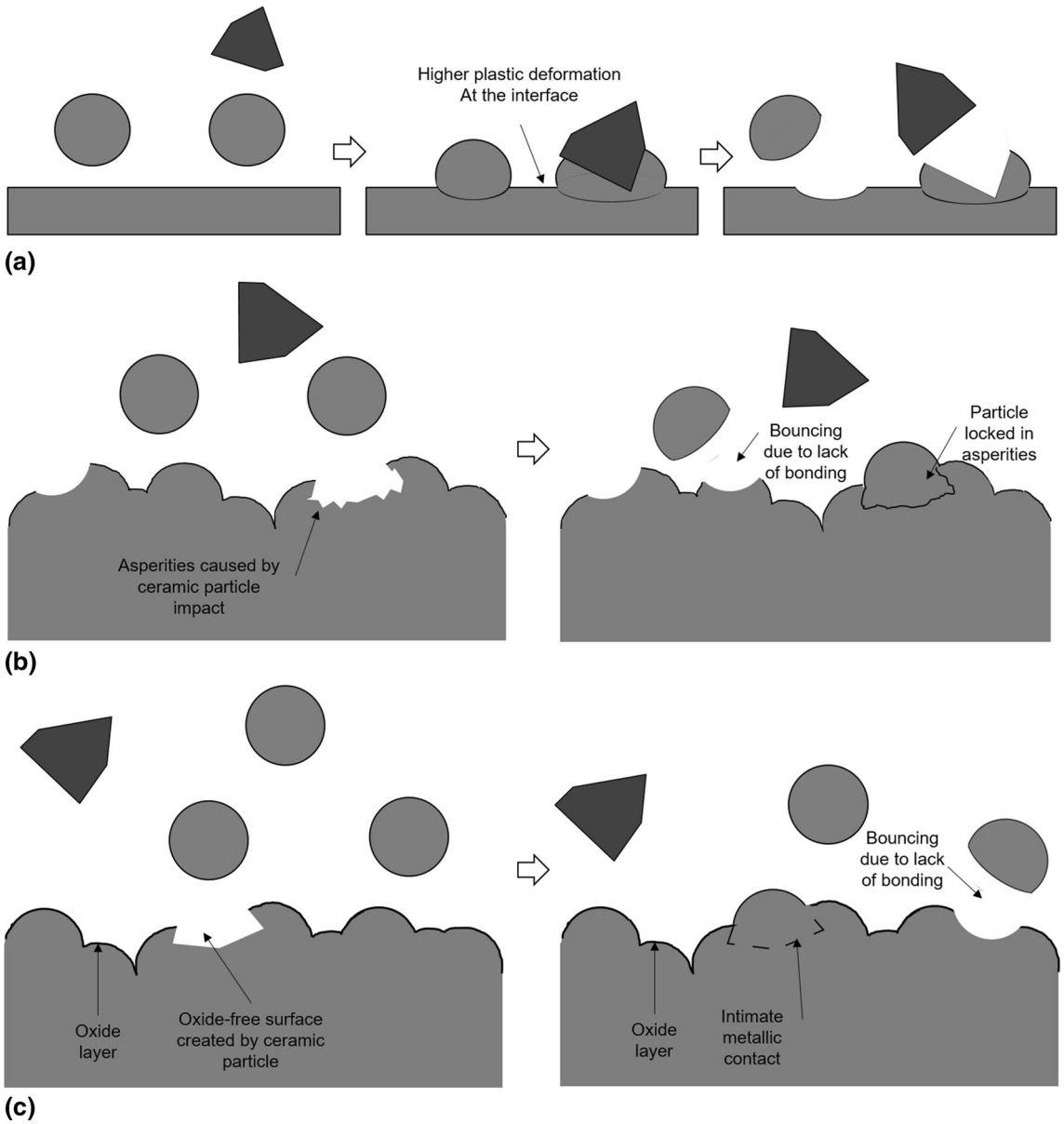

Fig. 1 Three mechanisms proposed in the literature for the DE increase in metal–ceramic mixtures: (a) Metallic particles adhere due to peening of ceramic particles upon impact; (b) metallic particles adhere mechanically due to the asperities created by previous ceramic particle impacts; (c) metallic particles adhere to oxide-free surfaces cleaned by previous ceramic particle impacts

20, 43, 44, 48). They described the different steps of erosion caused by hard angular particles impacting and cutting on a metallic surface. As explained, the process starts with a combination of embedment of the ceramic particles in the metal and cutting of the metal by the ceramic particles. Initially, the rate of embedment is higher than the rate of cutting, leading to a mass gain. This is followed by a saturation of the surface by the embedding particles. Then, the impacts break some of the superficial ceramic stabilizing its content; at this point, the embedment rate reaches zero, and the cutting rate leads to a mass loss in the entire substrate. Figure 2 shows an extract of the investigation, showing surface mass change caused by the impacting ceramic particles at different speeds.

In these studies, the substrate is impacted solely by ceramic particles, while in the case of cold spray, the substrate is bombarded by a combination of both metallic and ceramic particles. While the ceramic particles initially embed and eventually act toward erosion, the metallic particles that adhere will build a coating renewing the surface by a new non-eroded surface. Therefore, depending on the DE and the ceramic/metal ratio of the powder mixture, it is possible that the erosion state is never reached.

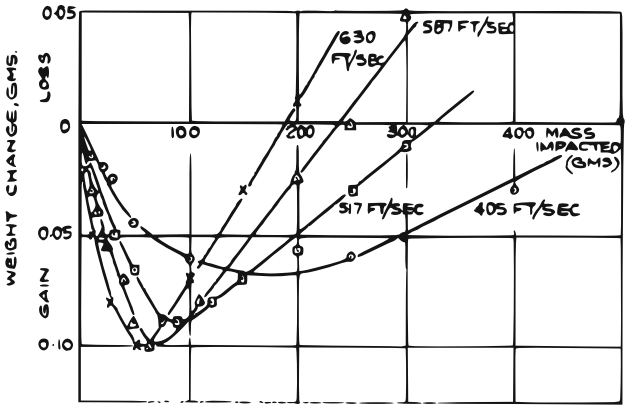

Fig. 2 Weight change for aluminum plates vs. mass impacted grit (Ref 44)

The focus of the present study was to verify and assess the fundamental mechanisms responsible for the increment in DE seen by the addition of ceramic particles in the feedstock powder. Commercially, pure aluminum and alumina were mixed and the influence of Al_2O_3 content on the DE was measured. The three potential mechanisms proposed in the literature for the increase in DE with the addition of ceramic particles investigated were: (1) the interaction between ceramic and the metallic particles upon impact, (2) the effect of the asperities created by the ceramic particle impacts, and (3) the effect of the oxide removal from the substrate. The effect of the interaction between ceramic and metal upon impact was analyzed by finite element analysis combined with a probabilistic analysis. For the effect of the asperities, the DE of a single layer of aluminum particles was measured. Finally, the effect of the oxide cleaning was evaluated as the complement of the other two effects.

Experimental Procedures

Materials and Mixtures

Commercially available pure aluminum powder (SST-A5001) (Centerline (Windsor) Ltd. Windsor, Ontario, Canada) was used. This is a gas-atomized powder with an irregular shape, as seen in Fig. 3(a).

Figure 4(a) presents the particle size distribution of this powder (measured using a Microtrac Particle Size Analyzer S3500, Nikkiso, Japan), revealing an average particle size of 26 μm. The ceramic powder utilized for this investigation was alumina powder (G-0001), also from Centerline. Morphology and particle size distribution of this powder can be found in Fig. 3(b) and 4(b), respectively. The alumina particles are angular, and the average particle size is 22 μm. In order to study the effect of different ceramic contents and influence on the deposition behavior during cold spray, a total of eleven aluminum–alumina mixtures were produced. Table 1 shows the samples designation name as well as the weight percentage and the volume proportion of each powder used in this investigation. The powders were weighed and mechanically blended for 10 min prior to deposition.

Cold Spray Deposition

The cold spray system used to produce the coatings for this work is the commercially available EP Series SST Low Pressure Cold Spray System (Centerline Ltd., Windsor, Ontario, Canada). The system consists of a 15 kW heater with a maximum gas temperature of 500 °C and a maximum gas pressure of 3.8 MPa. The De Laval nozzle used for this work has a throat diameter of 2 mm and a diverging section length and exit diameter of 120 and 6.6 mm, respectively. The mixed powder was fed using a commercially available rotatory powder feeder model AT-1200HP (Thermach Inc., Appleton, WI, USA). All coatings were sprayed using the spray parameters given in Table 2.

Coatings Characterization

The coatings produced with the different mixtures were characterized using several methods. Ceramic content measurements were taken using a digital microscope (VHX-1000, Keyence Corporation, Osaka, Japan) and contrast analysis. Imaging was performed on the coatings cross sections using the scanning electron microscopy (SEM) model EVO MA-10 (Carl Zeiss AG, Oberkochen, Germany), and composition was measured using an energy-dispersive x-ray spectroscopy (EDS) INCA X-Act (Oxford Instruments, Oxford, England). By using the overall DE, the feedstock powder composition, and the coating composition, it is possible to calculate the partial DE of aluminum and alumina (Ref 16). This allows to draw conclusions related to the increased DE of the metallic particles by segregating them from the effect of the mass contribution of the ceramic phase.

Erosion Tests

To ensure that the aluminum partial DE is evaluated properly, it is important to consider the effect of erosion that alumina might have on the aluminum particles. At higher alumina content in the feedstock powder, the ceramic particles may erode the aluminum phase, reducing the coating aluminum composition and therefore leading to a perceived lower partial DE of aluminum. If the state of the deposition is in the erosion zone, then the value can be corrected by knowing the erosion rate of the alumina

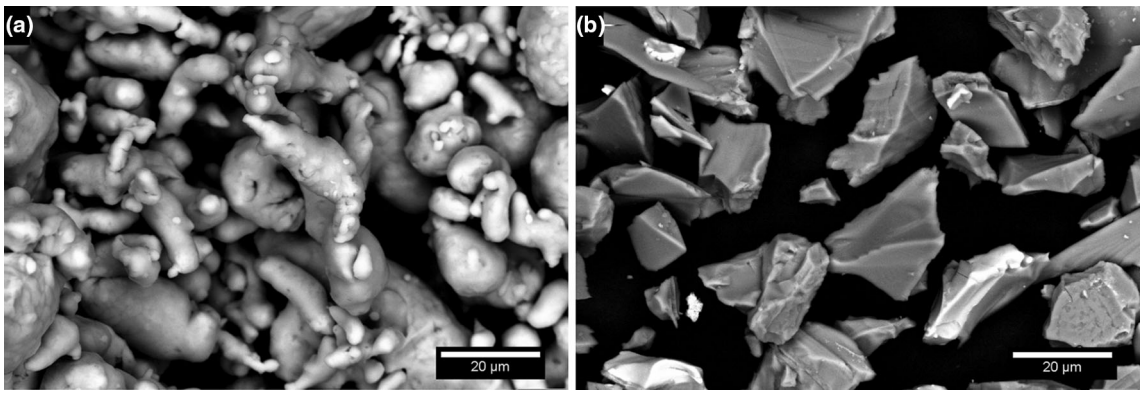

Fig. 3 Overview of feedstock particles used: (a) aluminum particles; (b) alumina particles

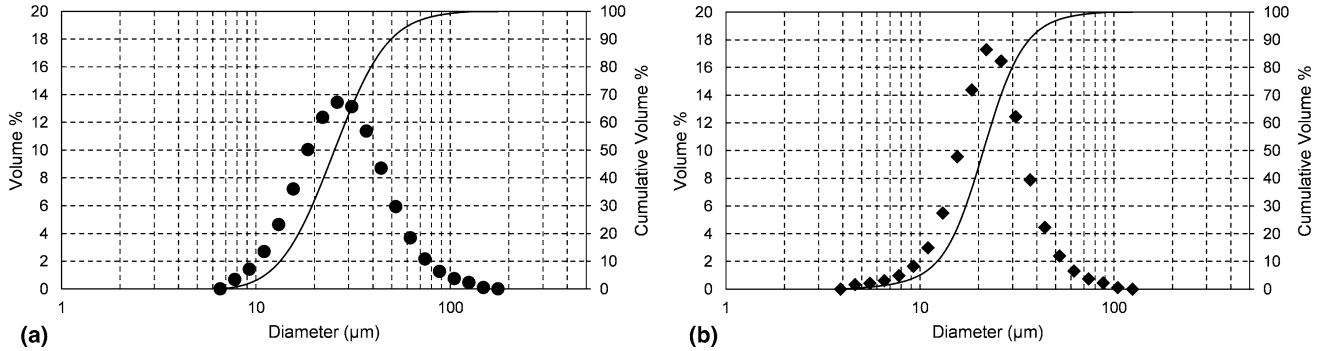

Fig. 4 Particle size distribution: (a) aluminum particles; (b) alumina particles

Table 1 Feedstock powder compositions

Composition designation	Feedstock powder Al wt.%	Feedstock powder Al_2O_3 wt.%	Feedstock powder Al vol.%	Feedstock powder Al_2O_3 vol.%
Al-00	100	0	100	0
Al-01	90	10	93	7
Al-02	80	20	85	15
Al-03	70	30	77	23
Al-04	60	40	69	31
Al-05	50	50	59	41
Al-06	40	60	49	51
Al-07	30	70	39	61
Al-08	20	80	27	73
Al-09	10	90	14	86
Al-10	0	100	0	100

particles in a cold spray aluminum coating. If the state of erosion has not been reached, no correction is needed. A similar approach than the one presented in a previous study (Ref 44) was used to determine the initial mass gain and the erosion rate of the deposition. In order to determine the erosion zone of alumina on an aluminum coating, a pure aluminum coating was impacted by a layer of pure alumina. The spray parameters were the same as the ones used to obtain the coatings but with a lower feed rate in order better control the amount of ceramic injected. Since

Table 2 Cold spray parameters

Parameter	Value
Gas temperature	250 °C
Gas pressure	1.65 MPa
Gas nature	Nitrogen
Traverse speed	20 mm/s
Passes	3
Feed conditions	320 holes wheel at 8 RPM
Standoff distance	15 mm
Substrate	Al-6061

erosion rate is the ratio between mass lost in the substrate and mass of ceramic sprayed (in mg/g), changing this parameter does not affect the substrate erosion behavior (Ref 44). This test allows assessing the erosion rate of the alumina particles on the deposited aluminum particles. With the erosion curve, the feedstock powder composition, and the DE of the spray, it is possible to estimate the amount of ceramic impacting the coatings, and the rate at which the surface is renewed with a new layer of aluminum. This leads to evaluate the erosion state of each feedstock powder during the deposition of the mixture and to assess the impact of erosion on the deposition.

Assessment of Deposition Efficiency Mechanisms

To evaluate the process DE, the powder feed rate was measured prior to each deposition. These measurements were taken three times to ensure consistency. The substrates were also weighed before and after deposition (using a precision scale Sartorius Extend—model ED124S, with a readability of 1 mg). The DE was calculated using Eq 1. The standard deviation was calculated using propagation of uncertainty (based on the uncertainty of weight change of the substrate, feed rate values, and weight measurements).

$$\mathrm{DE} = \frac{\Delta m_{\mathrm{s}}}{m_{\mathrm{i}}} = \frac{\Delta m_{\mathrm{s}} \cdot v_{\mathrm{n}}}{\mathrm{FR} \cdot d} \qquad \text{(Eq 1)}$$

In this equation, DE is deposition efficiency, m_{i} is the mass of powder injected into the nozzle, Δm_s is the change in mass of the substrate after deposition, FR is the feed rate of powder injected, d is the distance traveled by the nozzle on top of the substrate, and v_{n} is the speed of the nozzle relative to the substrate. Beside this overall DE, partial DEs where also calculated. Cross sections of the coatings produced were obtained, and ceramic content was computed by contrast analysis and also using EDS. Using the feedstock powder composition and the resulting coating compositions, it is possible to calculate the partial DE of each component.

Impingement of Ceramic Particles on Metallic Particles upon Impact

This proposed mechanism suggests that the DE increase might be caused by the impingement of the hard phase (alumina) on the soft phase (aluminum) upon impact (Ref 42). The direct observation of this phenomenon is challenging and potentially not currently possible, due to the small dimensional and time scales involved. However, some assumptions can be made in order to estimate the incidence of this phenomenon and its overall effect on DE. For this mechanism to be valid, a ceramic particle should impinge a metallic particle that would otherwise not adhere to the substrate/coating; this impingement makes it possible for the metallic particle to adhere, thus increasing the DE. The effect of the impingement of an alumina particle on an aluminum particle was studied using finite element analysis. The details of the simulation are explained in the following section. To assess the influence of ceramic particle impingement on the adhesion between aluminum particles and the substrate, the interface elements (aluminum particles–substrate) were analyzed using the outcomes of the simulation that might improve the bonding between them such as the plastic deformation, temperature field and stress produced.

Finite Element Analysis

A 2D finite element analysis was performed in order to evaluate whether the impingement of an alumina particle on an aluminum particle leads to phenomena that can promote the adhesion of the latter to the substrate. The software Abaqus/Explicit was used to carry this analysis. The modeling results of the impact of aluminum particles into an Al6061 substrate were compared with the modeling results of the impact of aluminum particles concomitant with an impact with a ceramic particle. Plastic deformation, temperature and contact pressure were compared at the substrate interface to assess whether the ceramic particle impact does promote bonding. These properties have been proposed to be indicators for the generation of metallurgical bonding and therefore an increase in DE (Ref 9, 47, 49, 50).

Cross sections of representative aluminum and alumina particles were digitalized in order to obtain the geometry required for the simulations. Three aluminum and two alumina particle geometries were chosen, and six different impact configurations were studied. The material properties used in the simulations for aluminum particles, Al6061 substrates, and alumina particles are shown Table 3.

Johnson–Cook constitutive equation (Eq 2) was used to model the plastic behavior of pure aluminum particles and A6061-T6 substrates, and the equation of state used was

the linear Us-Up Hugoniot form of Mie–Gruneisen (Eq 3). These equations have been used in several investigations to describe cold spray particle and substrate deformations (Ref 51-54). The equations are:

$$\sigma_{\text{eq}} = \left[A + B\varepsilon_{\text{p}}^{n}\right]\left[1 + C\ln\left(\frac{\dot{\varepsilon}_{\text{p}}}{\dot{\varepsilon}_{\text{ref}}}\right)\right]\left[1 - \left(\frac{T - T_{\text{ref}}}{T_{\text{m}} - T_{\text{ref}}}\right)^{m}\right] \quad \text{(Eq 2)}$$

$$p = \frac{\rho_0 c_0^2 \eta}{(1 - s\eta)^2}\left(1 - \frac{\Gamma_0 \eta}{2}\right) - \Gamma_0 \rho_0 E_{\text{m}}, \quad \eta = 1 - \frac{\rho_0}{\rho} \quad \text{(Eq 3)}$$

where A, B, C, n, m, $\dot{\varepsilon}_{\text{ref}}$, and T_{ref} are the Johnson–Cook parameters, ε_{p} is the plastic strain, $\dot{\varepsilon}_{\text{p}}$ is the plastic strain rate, T is the temperature of the material, and T_{m} is the melting point. In Eq 3, p is the hydrodynamic stress, ρ_0 is the initial density, ρ is the actual density, c_0 is the material speed of sound, s is the Hugoniot slope, Γ_0 is the Gruneisen constant, and E_{m} is the energy per unit mass. The parameters for the materials used can be found in Table 4.

The particle impact velocities required as model inputs were measured using a cold spray meter (CSM) eVOLUTION (Tecnar Automation Ltd, St. Bruno, Canada). The system performs in-flight diagnostic on individual particles illuminating the particles with a continuous 2.4 W ($\lambda = 810$ nm) laser and capturing the reflection through a dual split photomask in order to calculate the velocity. The substrate temperature used in the model was measured using a FLIR i7 Portable Infrared Camera. The particle impact temperature was assumed to be 80% of the gas stagnation temperature, similarly to what has been calculated in previous investigations (Ref 57, 58).

A quadratic mesh was used with a coupled temperature–displacement element type (CPE4RT). The maximum element size used was μm. Arbitrary Lagrangian–Eulerian (ALE) adaptive domain was used in the in the substrate and aluminum particle mesh. Equivalent plastic strain (PEEQ), temperature, and contact pressure (CPRESS) were evaluated in the elements at the surface of particle and coating (Ref 54). The results were averaged through the elements, and the maximums were used for the comparison.

Table 3 Material properties used in simulations

	Aluminum	Al6061-T6	Al_2O_3
k, W/m K	237	167	30
ρ, kg/m^3	2710	2710	3900
G, GPa	26	26	…
E, GPa	…	…	300
v	…	…	0.21
C_p, J/kg K	910	900	700

Probabilistic Analysis

The FEA results presented later show the possibility of increasing the chances of adhesion of an aluminum particle when a ceramic particle is impacting it. It is important to note that for this interaction to occur, the alumina particle must hit an aluminum particle before the latter bounces back. If the ceramic particle arrives too late, the aluminum particle will be long gone, and no impingement would occur. The short time span and narrow area that the ceramic particle has to hit to influence the aluminum particle impact make this event potentially unlikely. The probability of this event was calculated in order to evaluate the incidence of this potential mechanism on the overall DE. The probability equation used is shown in Eq 4:

$$\mathbb{E}_{\text{event}}(t) = [\mathbb{P}(p_1 = \text{Al}) \times [1 - \text{DE}(\text{Al})]] \times \mathbb{Q}(t) \times \mathbb{P}(p_2 = \text{Al}_2\text{O}_3) \quad \text{(Eq 4)}$$

where $\mathbb{E}_{\text{event}}(t)$ is the probability of the event (aluminum particle being impinged by alumina particle while it is impacting the substrate) to happen over a period of time t.

Table 4 Johnson–Cook and Mie–Gruneisen parameters used in simulations

Johnson–Cook parameter	Al-1100-H12 (Ref 55)	Al6061-T6 (Ref 56)
A (Mpa)	148.4	324
B (Mpa)	345.5	114
C	0.001	0.002
n	0.183	0.42
m	0.895	1.34
$\dot{\varepsilon}_{\text{ref}}$	1	1
T_{m} (K)	925	925
T_{ref} (K)	293	300
Gruneisen constant (Γ_0)	1.97	1.97
Speed of sound ($^m/_s$)	5386	5240
Hugoniot slope (s)	1.34	1.4

$\mathbb{P}(p_1 = \mathrm{Al}) \times [1 - \mathrm{DE}(\mathrm{Al})]$ is the probability of the first impacting particle to be an aluminum particle that would not stick to the substrate. $\mathbb{Q}(t)$ is the probability of at least one of the incoming particles impacting during a time span t to hit the area defined the first particle. Finally, $\mathbb{P}(p_2 = \mathrm{Al_2O_3})$ is the probability for that incoming particle to be an alumina particle. It is important to note that $\mathbb{Q}(t)$ takes into consideration the time span that the second particle has to impact the first particle, and the narrow area where it has to hit in order to have an interaction. $\mathbb{Q}(t)$ can also be written as:

$$\mathbb{Q}(t) = 1 - (1 - \mathbb{Z})^{N(t)}$$

This equation gives the probability of at least one of the incoming particles to peen the previous one in a specific time span. $N(t)$ represents the number of particles hitting the substrate in this time span t. $\mathbb{Z}$ is the probability of impacting inside a specific zone (in the vicinity of the previous particle). Therefore, $(1 - \mathbb{Z})^{N(t)}$ is the probability of all the incoming particles impacting outside this specific zone. Finally, the complement of this term represents the probability of not all the particles to hit outside this area (thus, at least one hits inside this area). It is important to note that $\mathbb{Z}$ represents the likelihood of an impact to happen in a specific area. This probability is different depending on the relative position from the nozzle axis. Directly below the nozzle, a higher flow rate of particles hits the substrate compared with a zone away from the nozzle; therefore, $\mathbb{Z}$ is higher at the center of the nozzle and decays toward the periphery.

The probability $\mathbb{P}$ was obtained based on the ceramic content of the feedstock powder. The total number of particles (aluminum and alumina) was calculated per unit mass using the density of the elements as well as the average particle size. For simplicity, the volume of a sphere was used to estimate the number of particles per unit mass. The probability $\mathbb{P}(p = \mathrm{Al})$ was considered as the calculated number of aluminum particles over the total number of particles in an unit mass. Similarly, $\mathbb{P}(p = \mathrm{Al_2O_3})$ was considered as the number of alumina particles over the total number of particles.

$N(t)$ was computed using the total number of particles per unit of mass of the powder mixture and the feed rate measured during deposition. A uniform number of particles per unit of time was assumed (constant feed rate). The time span t is the impact time of the aluminum particle from initial contact with the substrate until it has completely bounced back and is not in contact with the substrate anymore and was obtained from FEA simulations. Finally, to obtain the probability $\mathbb{Z}$, it was necessary to obtain the spatial distribution of particles impacting the substrate directly below the nozzle. The distribution of particles in the nozzle was assumed to be axisymmetric with a radial probability distribution profile. This distribution was fitted from a single coating spot produced by the nozzle. This curve was obtained using a 3D depth composition image (VHX-1000, Keyence Corporation, Osaka, Japan). It was assumed that the spot left by the nozzle closely represents the spatial particle distribution. With this radial distribution function, $\mathbb{Z}$ can be defined as the cumulative distribution function expressed by:

$$\mathbb{Z} = f[\boldsymbol{x_1} - \Delta_r < \boldsymbol{x_2} < \boldsymbol{x_1} + \Delta_r] \times \frac{\Delta_\theta}{\pi}$$

where f is the radial distribution of particles below the nozzle, $\boldsymbol{x_1}$ and $\boldsymbol{x_2}$ are the position of impact of the initial particle and second particle, respectively, Δ_r and Δ_θ are ranges of where the second particle can impact and still hit the previous particle. Δ_r was assumed as the addition of the average aluminum and ceramic radiuses, and Δ_θ is defined by the tangent arc of Δ_r and the distance from the nozzle axis. The area of interaction assumed by this equation is shown in Fig. 5(a) as a shaded area. The cumulative area of interaction of the function f is represented in Fig. 5(a), but this represents a ring around the axis of the nozzle. To consider the angular segment, a section of arc $2\Delta_\theta$ was considered over 2π section for the full ring, as shown in Fig. 5(b) which is reduced to the term $\frac{\Delta_\theta}{\pi}$, to represent the probability of impact in the angular section of the ring. It is important to note that it creates a larger zone of interaction than in reality (due to the corners in the figure outside $\boldsymbol{r_2}$), therefore overestimating the probability of the event to happen.

Effects of Asperities and Oxide Removal on DE

These two effects are closely linked, as both are caused by the impact of ceramic particles. When ceramic particles hit the substrate, it creates craters and new surfaces through deformation and cutting of the soft metallic phase. At the same time, during the impacts, the native surface oxide layer of the substrate breaks exposing oxide-free metallic surfaces, as the oxygen-free gas (working gas) prevents the oxidation of this newly created surface maintaining it clean until the arrival of the next particle. In order to evaluate the effect of surface asperities created during the deposition of ceramic particles, it is important to separate it from the influence of oxide removal occurring during the same process.

To decouple these effects and evaluate independently the effect of the asperities, it is imperative to evaluate the DE of the aluminum particles hitting a surface topography identical to the one present during deposition of the mixture. For this reason, a test was designed to calculate the deposition efficiency of a single layer of aluminum

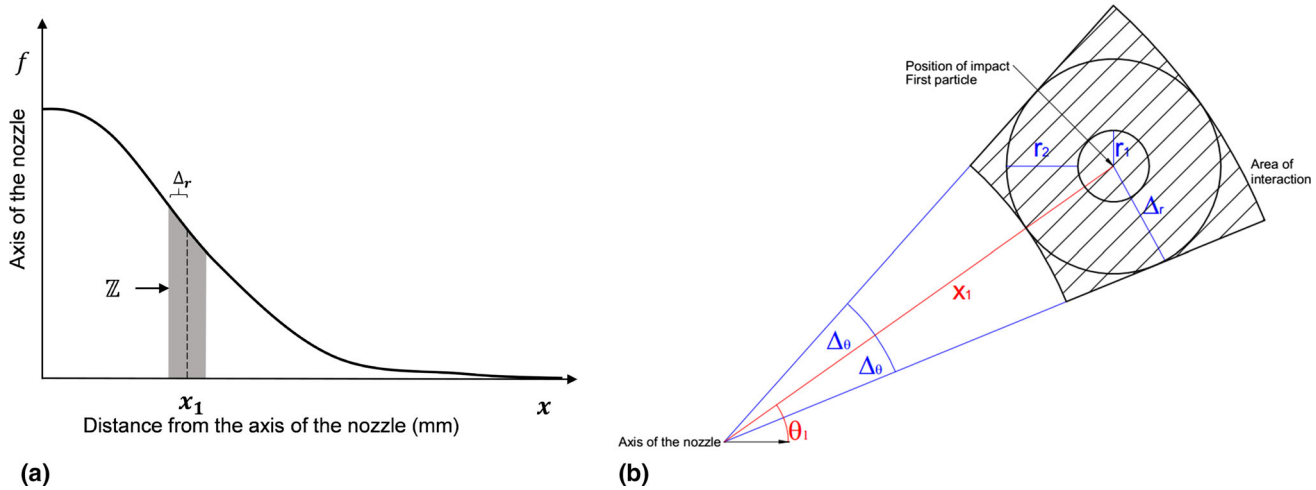

Fig. 5 Schematic of the impact zone for particles interactions: (a) radial distribution; (b) angular section

particles only. Properly designing this test for just a single layer of aluminum is crucial to evaluate solely the effect of asperities; otherwise, if more than a single layer is deposited, the second wave of particles will encounter a surface without the asperities skewing the measured DE toward the one of pure aluminum. To create the substrates with asperities, coatings were sprayed with each of the feedstock powder compositions using the parameters presented in Table 2. After deposition, the coatings were exposed to air at standard conditions for 72 h in order to develop the surface oxide layer. Particular care was taken in handling the samples in order not to affect the surface topology created during deposition.

Afterward, a single layer of pure aluminum particles was sprayed on top of the previously deposited coating. Spray parameters were kept constant, while feed rate was adjusted in order to obtain a single layer. The coatings were preheated with the working gas in order to closely recreate the same conditions of deposition.

This method allows segregating and assessing the contribution of the surface asperities created by the powder mixture on the DE of pure aluminum and indirectly allows to evaluate the contribution of the oxide layer removal. To directly assess the effect of the oxide-free surfaces without the asperities is a highly challenging task. Maintaining an oxide-free aluminum surface is a highly labor-intensive task and has to be done in an entirely oxide-free environment. For this reasons, the contribution of oxide-free surfaces in the DE was measured indirectly by subtracting the effect of the two other mechanisms studied in this investigation to the overall DE gain. It is important to mention that this method considered that the three mechanisms studied are the only ones acting toward the increment in DE in the deposition of ceramic–metal mixture.

Adhesion Strength and Mechanical Testing

Adhesion strength, hardness, and wear performance were measured for each coating produced. Adhesion strength was determined following the ASTM C-633 standard. A thermally cured elastomeric adhesive (FM-1000) with a tensile strength of 76.9 MPa was used. The samples were placed in an oven at 175 °C for 2 h to ensure the adhesive had properly cured. Testing was done using a universal tensile testing machine that recorded the force needed to remove the coatings. Three samples of each mixture were tested, and the mean and standard deviation of each preparation were computed. Hardness values were obtained using a Duramin-10 (Struers ApS, Denmark) equipped with a Vickers indenter using a load of 0.3 kgf. Wear tests were performed following the ASTM G133-05 standard. This dry slide wear test was conducted at three different travel lengths: 25, 50, and 100 m or until the wear track reaches the substrate. The load used was 25 N using a 3/16″ alumina ball.

Results and Discussion

Deposition Efficiency and Coating Characterization

The eleven powder mixtures were sprayed successfully, and DE measurements were completed. Figure 6 shows the DE for each of the powder mixtures. It is important to note that a coating was produced for each mixture where aluminum was present, even in the case of 90 wt.% Al_2O_3. This shows that the erosion rate inflicted by the alumina particles is low. The DE of pure aluminum was 11.0 ± 2.1% and increased up to 19.0 ± 2.5% for a 30 wt.% alumina content. From 30 wt.% of Al_2O_3, a

consistent decrease in DE is observed, reaching zero at 100% Al_2O_3. These results are in line with the literature, where similar behavior had been reported (Ref 16, 18, 19, 28, 40). This behavior (increase followed by a decrease) is evidence that there are two mechanisms competing, one to increase the DE of the mixture and another one to decrease it. At 30 wt.% Al_2O_3, the decreasing mechanism starts overcoming the increasing one, decreasing the DE.

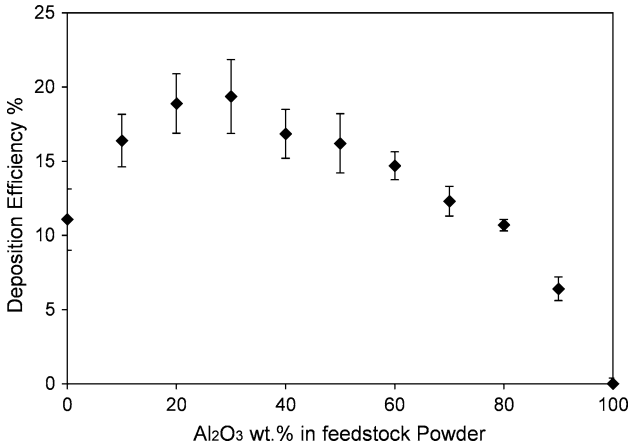

Fig. 6 Measured deposition efficiency of coatings for different feedstock powder compositions

Figure 7 shows some selected coatings cross-sectional images. It can be seen that the coatings are dense and the alumina particles appear to be embedded in the metallic phase.

Contrast analysis was used to compute the coatings ceramic content. The measured values were converted to wt.% to have a direct comparison. This analysis was also performed using x-ray spectroscopy (EDS). The values were converted to wt.% based on the oxygen content and assuming there are just aluminum and alumina phases present. Table 5 shows the alumina wt.% found in each of the coatings calculated using these two methods. These results can also be seen in Fig. 8, where it can be directly compared with the feedstock powder alumina percentage. It can be seen that the coatings alumina content is always lower than the one of the feedstock mixture. This result was expected due to the lower chances of deposition of alumina compared to the deposition of aluminum. The relation between the injected and deposited alumina appears to be linear, averaging to 51.2% of alumina retained when the coatings are formed. These values are similar to the ones reported in previous investigations (Ref 16, 18, 26, 29, 35, 40, 59), despite using different feedstock powders and cold spray systems.

The results in Table 5 were used to obtain the partial DE of aluminum and of alumina. This result is presented in

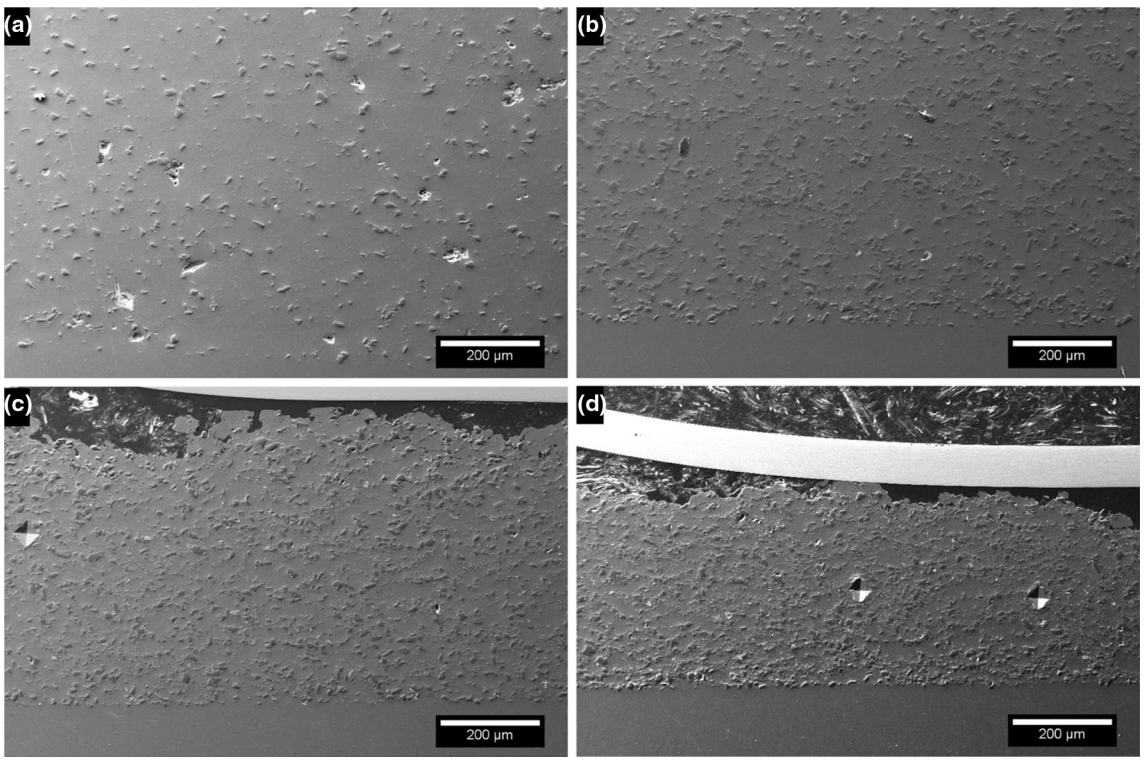

Fig. 7 Overview of coatings cross sections for feedstock powders containing: (a)10 wt.% Al2O3; (b) 40 wt.% Al2O3; (c) 60 wt.% Al2O3; (d) 80 wt.% Al2O3

Table 5 Alumina content in coatings measured by two different methods

Sample	Al_2O_3 wt.% in coating measured by contrast, %	Al_2O_3 wt.% in coating measured by EDS, %
Al-00	0 ± 0	1 ± 0
Al-01	9 ± 1	12 ± 0
Al-02	15 ± 1	16 ± 0
Al-03	22 ± 1	21 ± 1
Al-04	28 ± 2	26 ± 1
Al-05	30 ± 2	28 ± 3
Al-06	33 ± 2	30 ± 3
Al-07	39 ± 4	35 ± 1
Al-08	43 ± 4	38 ± 4
Al-09	51 ± 4	46 ± 3
Al-10	…	…

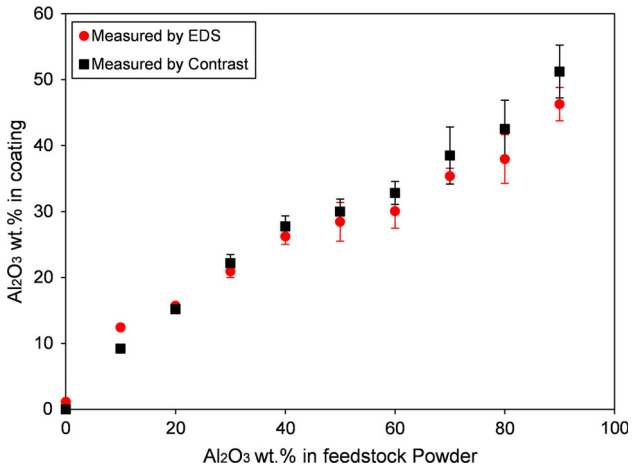

Fig. 8 Alumina content in coatings vs. alumina content in feedstock powders, measured by two different methods

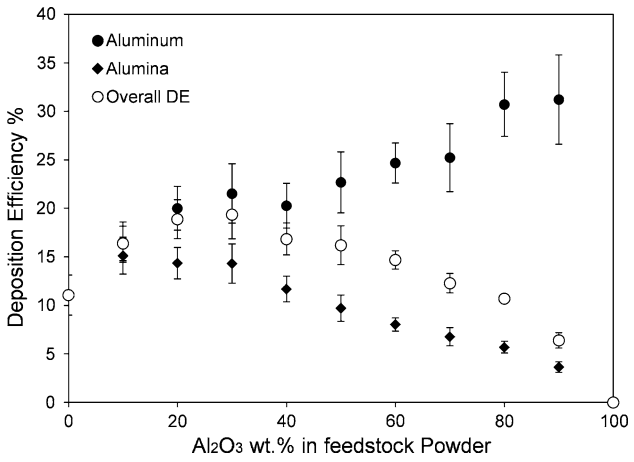

Fig. 9 Partial deposition efficiencies calculated using overall DE and alumina composition in coatings

Fig. 9. It is clear that the presence of alumina particles in the feedstock powder results in an increase in DE of the aluminum phase. This improvement increases with the alumina content present increasing the pure aluminum partial DE from 11.0% in pure aluminum to 31.0% for the 90 wt.% alumina mixture. The figure also shows that the alumina partial DE strongly depends on the feedstock powder aluminum content. Pure alumina has a DE of 0%, while 10 wt.% of alumina with 90% aluminum shows an alumina DE of 15.1%. Both powders get a benefit in DE under the presence of the other one. This interaction leads to a maximum overall DE at 30 wt.% alumina. The erosion test gives some insights on reasons behind the increment in alumina partial DE observed at higher aluminum content. The reasons behind the increase in aluminum partial DE are exposed with the assessment of the three potential mechanisms studied.

Figure 10 shows the substrate weight gain/loss versus the amount of ceramic impacting per unit area obtained from the erosion test. It can be seen that initially there is a substrate weight gain, reaching a maximum and followed by a constant decrease. This curve is similar to the one obtained by Neilson and Gilchrist (Ref 44) and reveals that before leading to erosion, ceramic particles first embed in the substrate, up to a certain level. The positive side of the curve represents the zone where alumina particles add mass to the substrate by embedding on it, and the negative side represents the cases when the particles erode the substrate, removing material from it. The point when the slope changes from positive to negative occurs when ceramic particles have reached a saturation limit of embedding, as an increase in the amount of particles directed toward the substrate results in removal of previously embedded particles. The slope of the negative side of the curve is the steady-state erosion rate and was evaluated 3.87 mg of eroded aluminum per gram of injected alumina.

The figure also shows an approximation of the erosion state experienced by aluminum while being sprayed for each of the feedstock powder compositions (vertical dotted lines). This is an estimated value based on the feedstock powders compositions, the feed rate, and the spray conditions. These values allow to calculate the mass per area of ceramic being sprayed in the time needed to renew a layer of aluminum. This time is calculated with the same values and the DE of aluminum at that composition (i.e., 0.62 mg/mm^2 of alumina will be sprayed in the time it takes to the aluminum to renew a mm^2 with a new layer).

It can be seen that even for 90 wt.% of alumina content, the state is still on the positive side of the curve. This suggests that at the spray parameters used, even the 90 wt.% of alumina content in the feedstock powder used does lead to a coating instead of erosion. This estimation is in line with the results obtained in the previous section, where

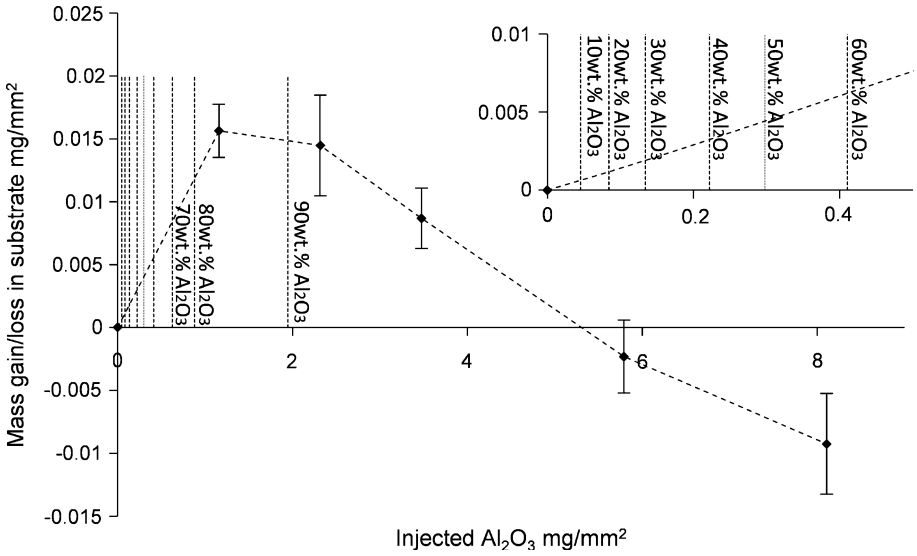

Fig. 10 Substrate mass change vs. alumina mass impacted for aluminum coatings. Vertical lines represent the equivalent injected mass per unit area of each feedstock powder mixture under the specific sprayed conditions

even the 90 wt.% alumina content powder produced a successful coating. The results also correlate well with alumina content measured by EDS at the surface of the coatings sprayed with each of the compositions, as presented in Fig. 11. The alumina composition at the surface increases consistently until it reaches a plateau at approximately 70-80 wt.% Al_2O_3 in the feedstock powder. This plateau could be a result of surface alumina saturation allowed to embed in the aluminum.

This test helps to explain the reasons behind the increment in DE seen by the alumina particles in the presence of aluminum. At higher aluminum content (lower alumina content), newly deposited metallic phase gets renewed more often than the erosion occurrences, lowering the chances of a ceramic particle to impact another embedded ceramic particle, increasing the chances to embed it in the metallic matrix staying in the coating, and therefore increasing its partial DE.

Interaction Ceramic–Metal upon Impact

Finite Element Analysis

This potential mechanism states that the increase in DE might be due to the peening of a ceramic particle into an impacting metallic particle that otherwise would not adhere. It has been proposed that this interaction will increase the particle/substrate deformation and therefore increase the probabilities of obtaining bonding via more favorable conditions at particle/substrate interface (Ref 18, 41, 42). A finite element analysis was performed to evaluate the potential of this process to increase the DE. Figure 12 shows the particles selected for the simulation and their digitalization. Three aluminum particles and two alumina particles were selected.

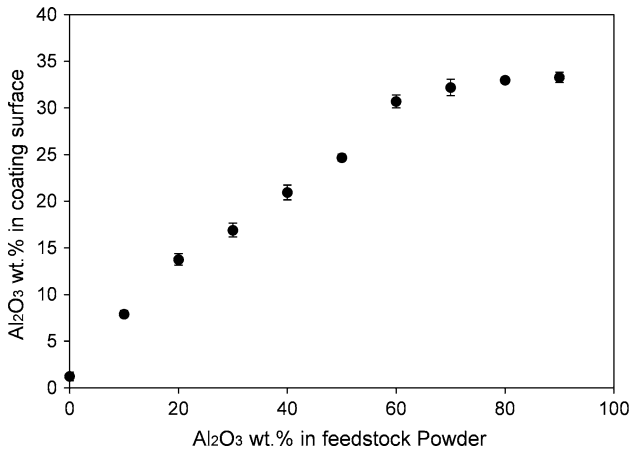

Fig. 11 Surface alumina content in coatings sprayed with different feedstock powder compositions

Figure 13(a) shows an example of one of the layouts used to perform the simulations. Each alumina particle was positioned to impinge each of the three aluminum particle with a total of six different simulations of aluminum–alumina interactions.

Laser diagnostic was used to assess the average particles impact velocities and was evaluated at 457 m/s for the aluminum particles and 451 m/s for the alumina particles. The substrate temperature measured was 105 °C, and the particle impact temperature was assessed as 145 °C. Figure 13(b) and (c) shows the results of one of the simulations. Table 6 shows the average increase in PEEQ, temperature, and CPRESS at the aluminum and substrate interface as a result of the ceramic particle impingement compared to the values computed in the aluminum particles without impingement of the ceramic particle.

The simulations show that the addition of an impinging ceramic particle increases the three properties. The contact

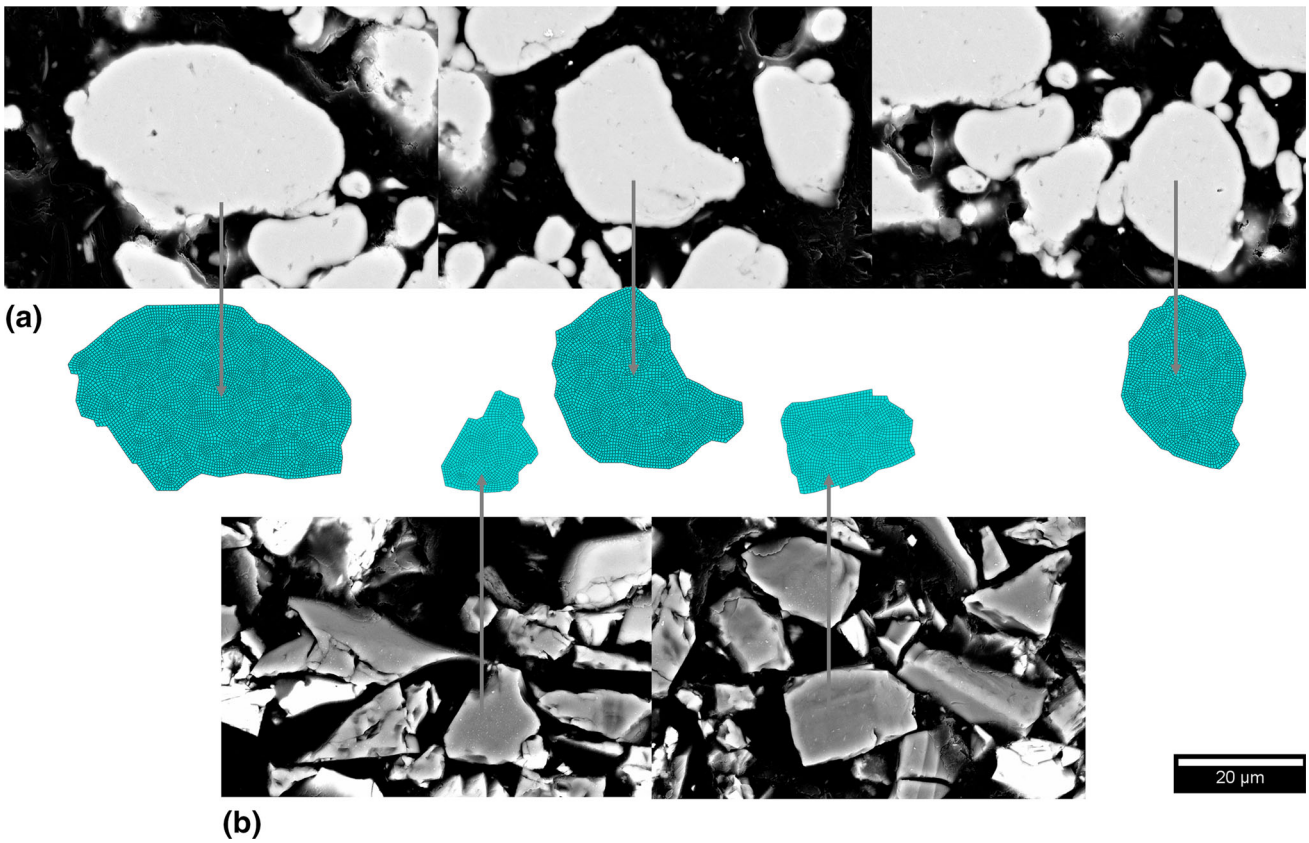

Fig. 12 Digitalized particles: (a) aluminum and (b) alumina

pressure between the substrate and the aluminum particles increased an average of 30% when an impinging alumina particle was added to the simulation. The plastic deformation showed an increment of nearly 60% in the aluminum particle, while the increment at the substrate was considerably lower at around 10%. Temperatures appeared to be the least affected by the addition of an alumina particle showing an average increase in the interface between the aluminum particle and substrate of 9%. Considering that the three properties increased with the addition of an alumina particle impinging an aluminum particle, it can be concluded that the conditions to get bonding are enhanced with the presence of an impinging ceramic particle.

Probability of the Event

The FEA results showed that if an alumina particle is peening an aluminum particle, the chances for the latter to adhere to the substrate increases. In this section, the likelihood of this peening event to happen during the impact time (the time the aluminum particle is in contact with the substrate prior to rebounding away if no bonding occurs) is estimated. As described before, the probability of this event is:

$$\mathbb{E}_{event}(t) = [\mathbb{P}(p_1 = Al) \times [1 - DE(Al)]] \times \left[1 - (1 - \mathbb{Z})^{N(t)}\right] \times \mathbb{P}(p_2 = Al_2O_3)$$

Based on the particle size distribution and mixture composition, the probability $\mathbb{P}$ was calculated. The number of particles impacting the substrate per second was calculated using the feed rate, the density of the materials, and the average particle size. These results are shown in Table 7. It is important to specify that the impact rates shown represent the total number of aluminum and alumina particles.

The radial distribution function $\mathbb{Z}$ was obtained. Figure 14(a) shows the 3D image of a single coating spot obtained. The height data from the center of the image composition were used to fit a Gaussian distribution (Ref 60). Figure 13(b) shows the fitted distribution function ($\mu = 0, \sigma = 1.7016$ mm). Having a normal distribution representing the probability density function of particles has the advantage of simplifying the cumulative function to:

$$\mathbb{Z} = \left[erf\left(\frac{x_1 + \Delta_r}{\sqrt{2}\sigma}\right) - erf\left(\frac{x_1 - \Delta_r}{\sqrt{2}\sigma}\right)\right] \times \frac{\Delta_\theta}{\pi} \qquad \text{(Eq 5)}$$

The impact time span was estimated, based on the FEA results and evaluated as $t = 0.1$ µs. This value is

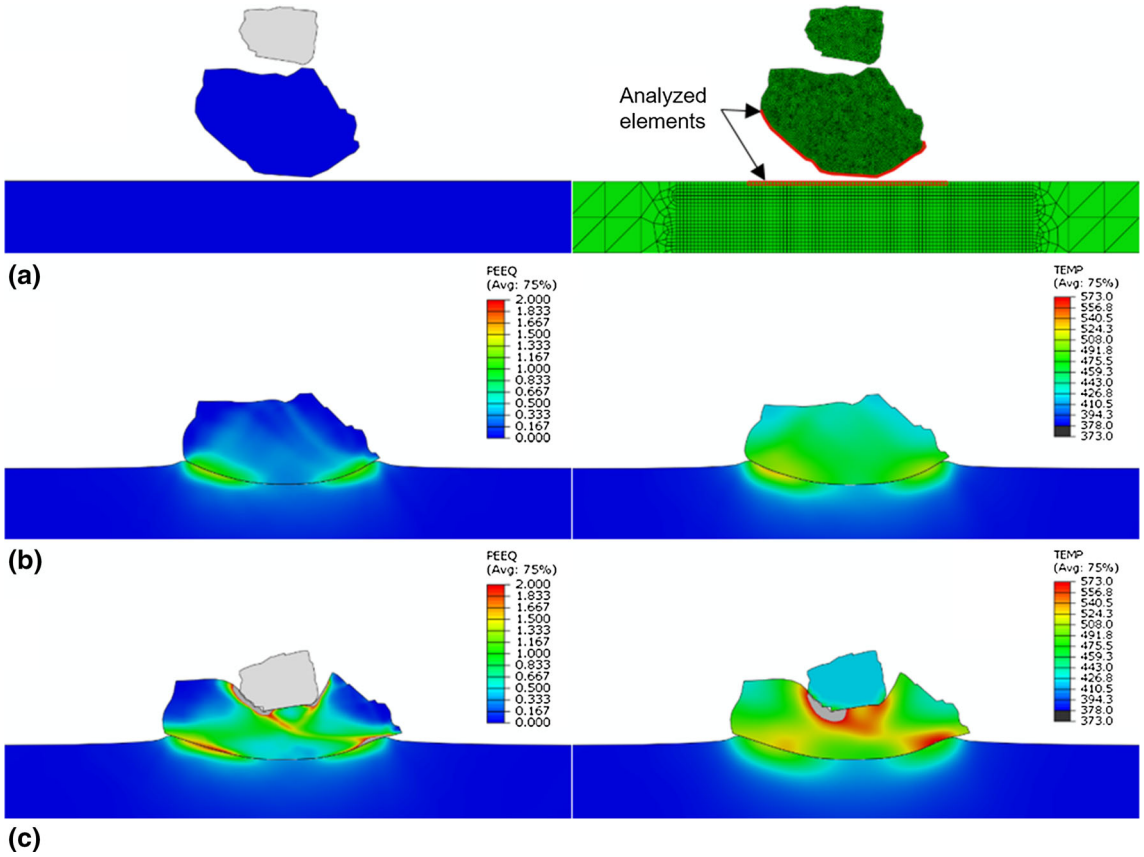

Fig. 13 (a) Layout of the simulations and elements analyzed; (b) aluminum impact: PEEQ and temperature; (c) aluminum–alumina impact: PEEQ and temperature

Table 6 Increases in CPRESS, PEEQ and temperature over values obtained in single aluminum impact

	CPRESS, %	PEEQ, %	Temperature, %
Aluminum particle	30.7 ± 12.7	59.6 ± 33.5	9.1 ± 4.1
Substrate	35.7 ± 9.7	9.2 ± 2.8	8.6 ± 5.9

considered conservative, as in the simulation the particle is already detached from the surface at that time, as shown in Fig. 15. Finally, the probability to obtain the event for some selected mixture along the spray radius is shown in Fig. 16. It is possible to see that the event is most probable at the center of the nozzle, and the highest probability occurs for the feedstock powder AL-05. At composition lower than 50 wt.% Al_2O_3 there are lower chances of getting an alumina particle to peen an aluminum particle, and at higher composition the chances of obtaining the first aluminum particle are also lower. The highest probability value obtained is 0.082%. It is important to note that this event considers the total flow of particles impacting the substrate, and in spite of the 6.5 million particle per second impacting the substrate the short time span for the event

Table 7 Calculated probabilities $\mathbb{P}(\mathbf{Al})$, $\mathbb{P}(\mathbf{Al_2O_3})$ and impact rate for each feedstock powder composition, for the specific spray parameters used

Mixture	$\mathbb{P}(Al)$, %	$\mathbb{P}(Al_2O_3)$, %	$N \times 10^6 par/s$
AL-00	100	0	5.12
AL-01	89	11	5.32
AL-02	78	22	5.81
AL-03	67	33	5.72
AL-04	57	43	6.19
AL-05	47	53	6.57
AL-06	37	63	6.97
AL-07	28	72	6.97
AL-08	18	82	6.98
AL-09	9	91	7.06
AL-10	0	100	7.14

and the narrow area keeps the probability value remarkably low.

Even though the FEA model shows that this interaction can increase the DE, the likelihood of the event indicates that the effect is negligible. Even with a conservative approach, the probability of this event in the most likely

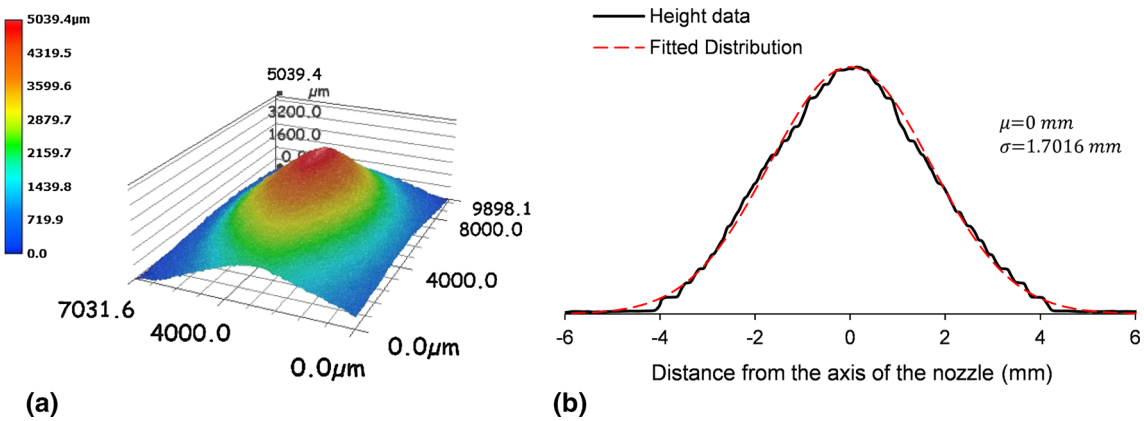

Fig. 14 (a) 3D image composition of a single spot; (b) adjusted distribution of particles to the profile

Fig. 15 Aluminum particle at 0.1 ms after the impact

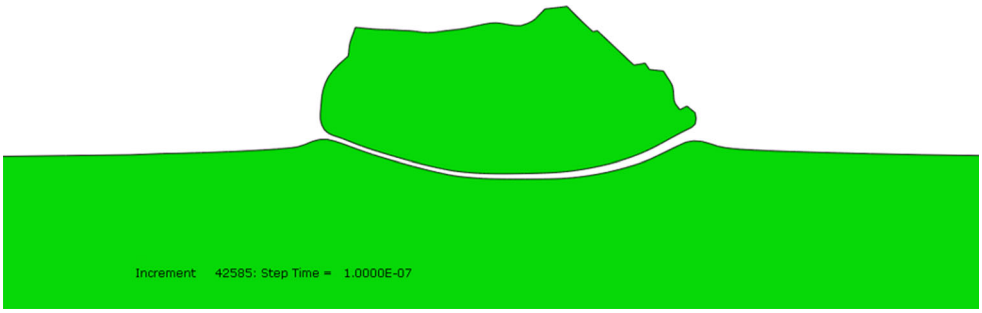

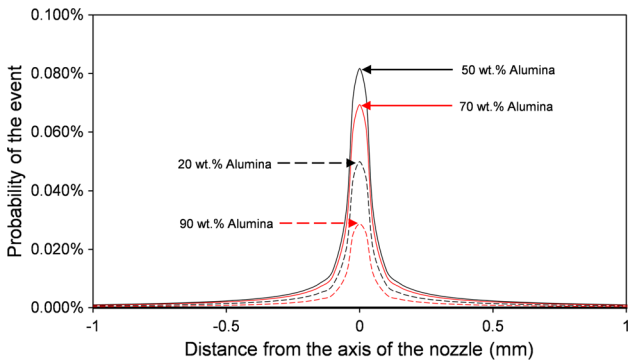

Fig. 16 Selected probability curves of an alumina interacting with aluminum upon impact

scenario is 0.082%. This value also represents the upper limit of the DE increment of this mechanism. Therefore, this mechanism cannot explain the increase in DE obtained in this work.

Effect of Asperities and Oxide Removal

Based on the previous section, it is possible to assume that the contribution of metal–ceramic interaction upon impact is negligible. The remaining possible mechanisms are related to the influence of the ceramic particles into the substrate, specifically, the effect of asperities created by the ceramic particle impacts, and the effect of oxide removal that the ceramic particle induces on the substrate surface once it impacts it. Figure 17 shows representative images of the coatings surfaces produced using feedstock powder with various alumina contents. It shows the creation and evolution of a number of asperities at different compositions. It can also be seen that the asperities are caused by the cutting of the metal and bouncing off of the sharp angular ceramic particles. The asperities dimensions are in the micron-sized range and appear to get smaller and more numerous as the wt.% Al_2O_3 of the powder increases; see highlights in Fig. 17. This result is expected as a higher number of ceramic particles impacting the surface leads to an increase in the number of new surfaces being generated, but these particles also deform asperities created by previous impacts, reducing their size.

The proposed mechanism states that the increase in DE occurs due to an increase in mechanical bonding between the aluminum particles and the surface due to more preferential sites allowing this to occur. Figure 18 shows an etched cross section of a coating, where the particles interfaces reveal locations where asperities might have acted to enhance mechanical interlocking.

The processes of oxide removal and asperities were decoupled by calculating the DE of a single layer of pure aluminum deposited on a coating surface produced with the

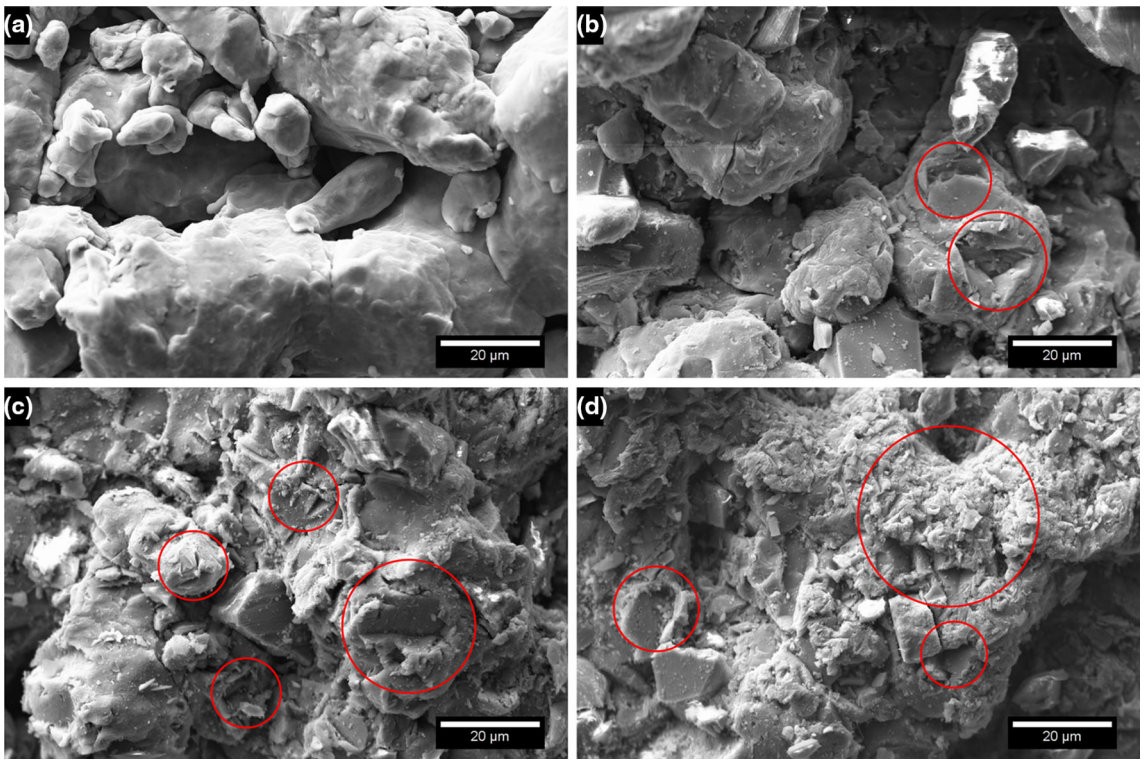

Fig. 17 Coatings surfaces, highlighting asperities in samples (a) Al-00 (b) Al-02 (c) Al-04 (d) Al-06

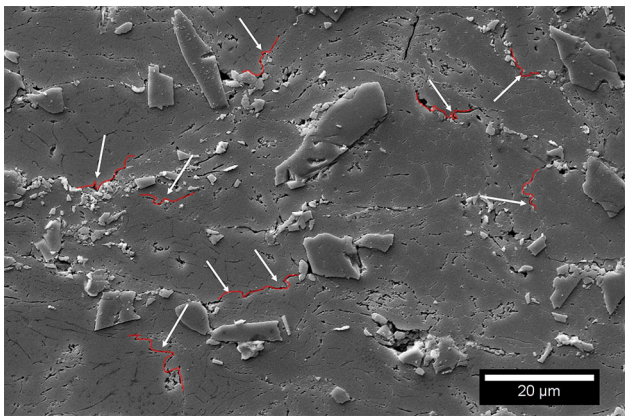

Fig. 18 Etched cross section of sample Al-06. Possible points of asperities locking particles are highlighted

different feedstock powders, and therefore with the asperities. The oxide layer was left to grow back on these coatings for 72 h. Figure 19 presents selected coatings cross sections showing the single layer of aluminum particles obtained during deposition on the previously sprayed aluminum–alumina coatings. Figure 20 displays the DE of these single layers of aluminum as well as the partial DE of aluminum calculated from overall DE and cross sections. The figure presents a positive influence of the asperities on the DE, increasing to 18%. Due to the exposure to normal conditions, the surface of the coatings is covered by the native oxide present in aluminum materials. Therefore, the effect that an oxide-clean surface due to the presence of alumina might have on DE is completely suppressed, and the increment in DE can only be attributed to the presence of those initial asperities. As Fig. 17 shows, a higher content of Al_2O_3 particles in the feedstock powder leads to a higher density of asperities on the surface of the substrate and already deposited particles; this leads to a higher DE of aluminum particles at higher alumina composition. It is important to note that the effect of asperities appears to reach a plateau, starting at 50 wt.% of Al_2O_3. This can be a result of the reduced asperity size at higher alumina composition.

Although the increase in DE due to asperities follows a clear trend, the asperity mechanism does not completely explain the increment in the partial DE of aluminum particles during the deposition of the mixture. The partial DE observed in the deposition of the mixture showed an increment from 11 to 31%, while the single layer deposition showed an increment to 18%. Therefore, it is evident that the presence of asperities is not the only mechanism acting to increase DE. The remaining increase in partial DE of aluminum particles is attributed to the last proposed mechanism, the oxide removal during deposition. As the number of asperities increases with the alumina content, the effect of oxide removal also appears to be increasing.

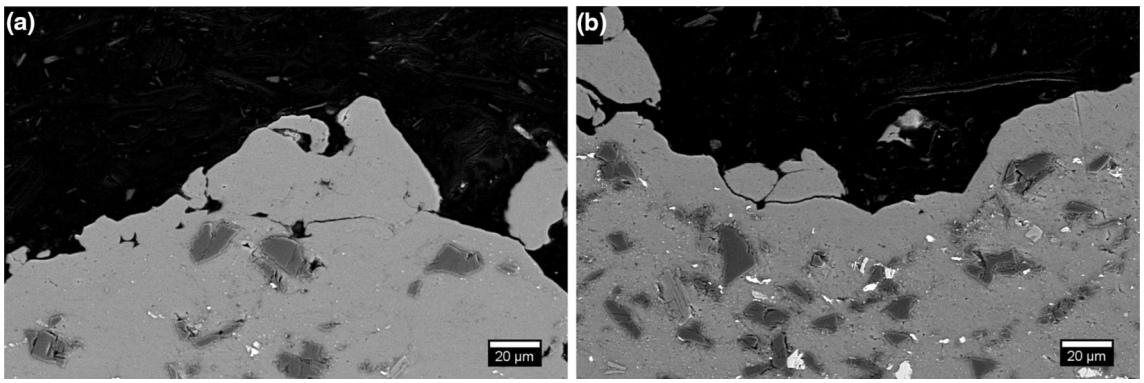

Fig. 19 Selected cross sections of a single layer of aluminum particles deposited on samples (a) Al-02 and (b) Al-06

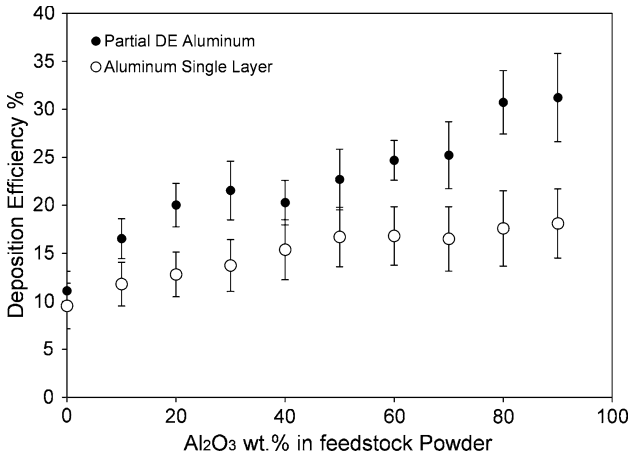

Fig. 20 Partial deposition efficiency of aluminum and of single-layer aluminum at different feedstock powder compositions

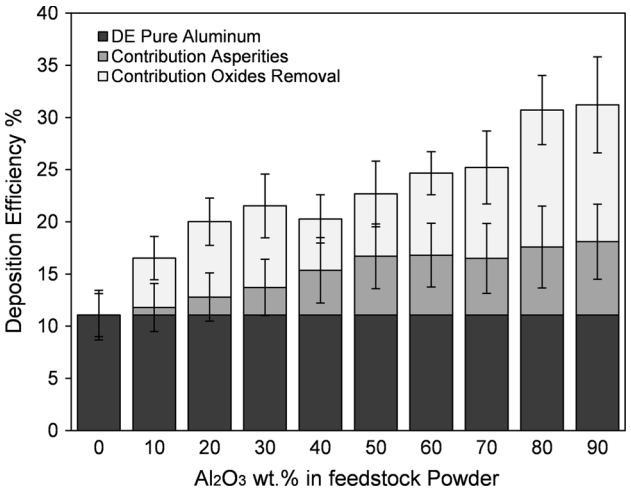

Fig. 21 Partial deposition efficiency of pure aluminum at different feedstock powder compositions showing the effect on DE of asperities and oxide removal over DE of pure aluminum

Both mechanisms seem to be very relevant in increasing partial DE of aluminum particles in the spraying of these mixtures as it is represented in Fig. 21. In this figure, the partial contribution of each mechanism is shown over the base DE seen in the deposition of pure aluminum. It is important to notice that Fig. 21 illustrates the contribution of each mechanism brought by the presence of ceramic particles in the feedstock powder.

An aspect to take into consideration is the morphology of the ceramic. In this study crushed alumina particles were used, and this powder has an angular morphology that promotes the creation of asperities. Similar tests should also be performed using spherical alumina, to suppress or change the asperities produced by the ceramic impacts. This is expected to alter the contribution of this aspect on the DE of the feedstock powder. Also, it is important to mention that the oxide cleaning mechanism is proved under the assumption that no other mechanism is acting toward the increment in DE. If another mechanism is discovered in future investigations, then this mechanism should have to be taken into account in order to re-evaluate the effect of oxide cleaning.

Mechanical Properties and Adhesion Strength

Table 8 shows coating hardness and the estimated hardness based on coatings composition and on the lower bound rule of mixtures, shown in Eq 6, where H_c is the hardness of the coating, v is the alumina volume composition of the coating, $H_{Al_2O_3}$ is the hardness of alumina (2500 Hv), and H_{Al} is the hardness of a pure aluminum coating (Ref 26, 27, 59, 61, 62); this relation accounts for the load sharing of distributed particles in a matrix. As expected, the hardness is strongly related to the coating ceramic composition; this relationship can be easily seen in Fig. 22 where coating composition is plotted against the hardness measured. The estimated hardness values were also plotted in this figure. It can be seen that the coating hardness is higher than the estimated value by the lower bound rule of mixture; this difference is expected as cold spray coatings have an intrinsic higher hardness due to cold working. At coatings with higher alumina composition, this difference gets larger as more ceramic particles impact and do not

Table 8 Measured and estimated hardness of coatings

Sample	Hardness $HV_{0.3}$	Estimated hardness
AL-00	45.0 ± 8.9	45.0
AL-01	52.3 ± 1.3	48.2
AL-02	64.4 ± 1.6	50.2
AL-03	68.5 ± 2.8	53.0
AL-04	72.3 ± 7.1	54.4
AL-05	78.1 ± 5.7	56.9
AL-06	79.9 ± 4.3	59.6
AL-07	86.1 ± 8.1	64.3
AL-08	89.5 ± 3.9	65.4
AL-09	114.2 ± 12.1	78.6
AL-10	…	…

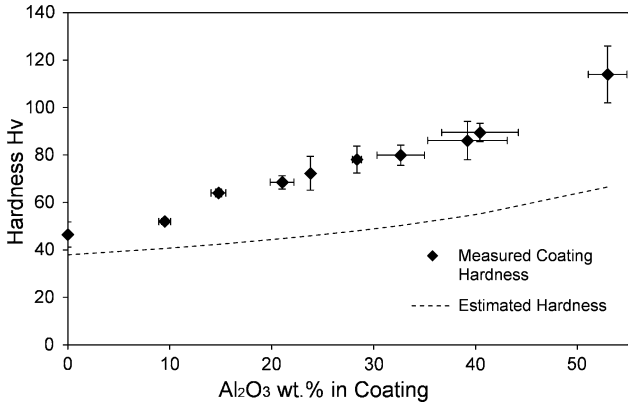

Fig. 22 Measured and estimated hardness of coatings vs. coating alumina contents

adhere into the coating, further increasing coating work hardening.

$$H_c = \left[\frac{1-v}{H_{Al}} + \frac{v}{H_{Al_2O_3}}\right]^{-1} \quad \text{(Eq 6)}$$

Wear test results are shown in Fig. 23. It shows the volume loss of each sample for a travel distance up to 100 m or until the coating was completely worn out. It is easy to see the strong dependence of the ceramic content on the coatings wear resistance. The figure shows three behaviors depending on the coating composition. Coatings with 22 wt.% Al_2O_3 content or less show almost no benefit in wear resistance compared with the pure aluminum coatings produced. Samples wore to the substrate in a distance travel lower than 5 m. Coatings with composition between 26 and 33 wt.% Al_2O_3 showed a sharp increase in wear resistance with ceramic content and extended to 100 m of travel distance without reaching the substrate. Finally, the last behavior seen starts with coating composition of 39 wt.% of Al_2O_3. These samples showed the highest wear resistance in the study, and no significant increment in resistance is observed in samples with alumina content above 39 wt.%. The coatings wear properties appear to have stabilized at this ceramic content level. This wear resistance dependence on the coating composition is common in metal matrix composites (Ref 1, 2, 27, 40). Ceramic particles, besides resisting the wear, help to distribute the stress throughout the material. For compositions with lower ceramic content, this stress distribution does not occur efficiently as the ceramic particles are too spread throughout the coating. The ductile phase deforms excessively and plows the ceramic particles as the wear tip slide through the coating, resulting in little wear resistance provided by the ceramic content. This mechanism changes at higher ceramic content, as the stresses get more distributed and the metallic phase does not suffer as much deformation, and the ceramic can act as a wear-resistant material (Ref 32, 40, 62, 63).

Finally, the adhesion test results can be seen in Fig. 24 where the adhesion strength is shown as a function of the feedstock powder composition. It is clear that the addition of ceramic particles into the feedstock powder greatly increases the coatings adhesion strength. Sample AL-00 showed an average adhesion strength of 18.6 MPA, and this value increases to values higher than the glue limit (above 70 MPa).

Irissou et al. (Ref 16) have also demonstrated the same behavior as the one seen in Fig. 24. They explained this increase in adhesion by the presence of asperities at the interface, increasing the mechanical bonding between the coating and the substrate. This is supported by this study. However, it is unlikely that mechanical bonding could improve the adhesion strength from 18 MPa to values higher than 70 MPa. It is also important to note that asperities are not the only acting mechanism. It was shown that DE might also be increased by oxide removal, increasing the chances of creating metallurgical bonding. This mechanism also can occur at the coating–substrate interface, considerably increasing the adhesion strength. This result supports the influence of oxide cleaning effect in the increment in DE explained in this study as the combination of these two mechanisms can account for this significant increase in adhesion strength. It is important to note that the adhesion strength appears to have a plateau between specimens Al-04 and Al-06. This behavior is in line with a similar plateau seen in the DE increment related to asperities. These two observations suggest that at higher ceramic compositions, the oxide cleaning effect might be more relevant and that the asperities effect gets saturated, but further investigation should be done in order to quantify the effect of each mechanism better.

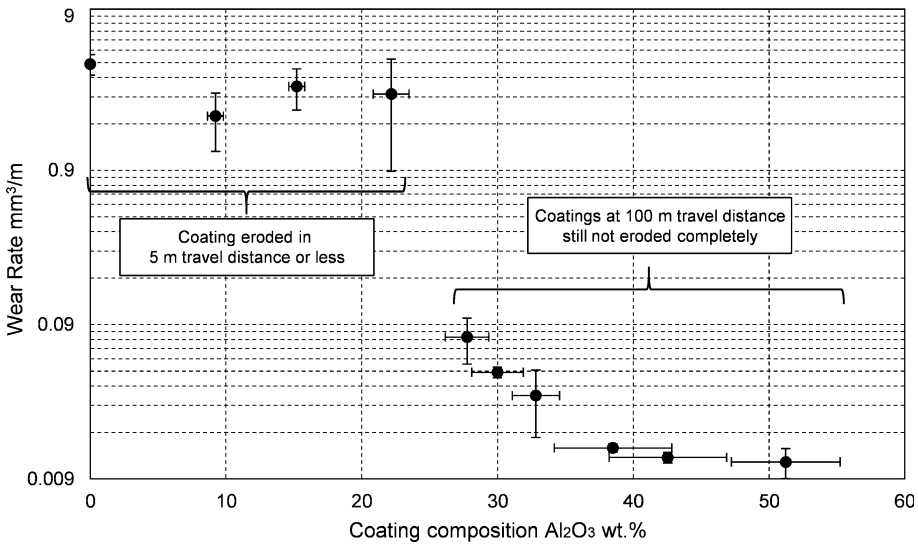

Fig. 23 Wear rate of coatings with different alumina contents, calculated until 100 m or worn to the substrate

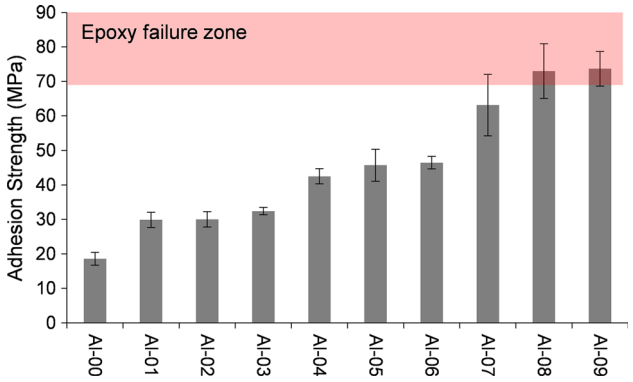

Fig. 24 Adhesion strength of coatings sprayed with different feedstock powder compositions

Conclusions

This study gives some insights into the production of cermet coatings and helps to understand behaviors previously observed in other investigations. The deposition behavior and effect of feedstock powder ceramic content were analyzed using eleven aluminum–alumina feedstock powder compositions. The DE of each of the composition was measured and revealed an increment in DE with the addition of ceramic content peaking at 30 wt.% followed by a consistent decrease reaching 0% DE at 100% Al_2O_3. The coatings composition revealed that even though the DE decreased at higher Al_2O_3 content, the partial DE of aluminum always increases, confirming that the presence of alumina particles in the flow has a positive effect on the deposition behavior of the aluminum particles. Three different potential mechanisms explaining this behavior were found in the literature and were assessed.

The interaction of ceramic and metallic particles upon impact was studied, showing that an impinging ceramic particle on aluminum particle leads to an increment on pressure, plasticity, and temperature at the aluminum–substrate interface, which might lead to higher chances of deposition of the metallic particle. However, a probabilistic analysis showed that the event is extremely unlikely and thus this effect can be considered negligible. Two other possible mechanisms were studied, namely the effect of asperities and oxide removal. This was done by measuring the DE of a single layer of pure aluminum particles over coatings previously deposited with the different feedstock powder. This showed that both asperity creation and oxide layer removal mechanisms have a major influence in the increment of DE during deposition.

Coatings cross section revealed that almost half of the ceramic content of the feedstock powder is lost but do contribute to coating formation by peening the coating and creating the asperities as well as influencing the coating hardness. Wear resistance was shown to benefit from ceramic content. Three zones of wear resistance were found. In coatings containing 22 wt.% of less of alumina, no significant benefit was seen. At higher values, a consistent increase in wear resistance is seen until 39 wt.% of Al_2O_3. Coating with higher alumina content did not show an increment in wear resistance. Adhesion strength of the coatings also increased with the addition of ceramic particles to the feedstock powder, reaching glue values with coating sprayed with a mixture with 70 wt.% of alumina or more. This can be explained by the asperities promoting mechanical bonding. Oxide removal is also potentially increasing the adhesion strength by promoting the probabilities of obtaining metallurgical bonding between the particles and the substrate.

References

1. J.R. Tinklepaugh, *Cermets*, Reinhold Publishing Corporation, New York, 1960
2. J.L. Ellis and C.G. Goetzel, Cermets, "*ASM Handbook Volume 2: Properties and Selection: Nonferrous Alloys and Special-Purpose Materials",* ASM International, Geauga County, 1990, p 1328.
3. C.P. Bergmann and J. Vicenzi, *"Protection against Erosive Wear Using Thermal Sprayed Cermet", Climate Change 2013—The Physical Science Basis*, Springer, Berlin, 2011
4. A. Evans, C. San Marchi, and A. Mortensen, *Metal Matrix Composites in Industry: An Introduction and a Survey*, Kluwer Academic, Dordrecht, 2003
5. R.C.C. Dykhuizen and M.F.F. Smith, Gas Dynamic Principles of Cold Spray, *J. Therm. Spray Technol.*, 1998, **7**(2), p 205-212
6. A.O. Tokarev, Structure of Aluminum Powder Coatings Prepared by Cold Gasdynamic Spraying, *Met. Sci. Heat Treat.*, 1996, **38**(3), p 136-139
7. A.P. Alkhimov, A.N. Papyrin, V.F. Kosarev, N.I. Nesterovich, and M.M. Shushpanov, *"Method and Device for Coating,"* Patent EP0484533 B1, 1995.
8. H. Assadi, F. Gärtner, T. Stoltenhoff, and H. Kreye, Bonding Mechanism in Cold Gas Spraying, *Acta Mater.*, 2003, **51**(15), p 4379-4394
9. T. Schmidt, H. Assadi, F. Gärtner, H. Richter, T. Stoltenhoff, H. Kreye, and T. Klassen, From Particle Acceleration to Impact and Bonding in Cold Spraying, *J. Therm. Spray Technol.*, 2009, **18**(5-6), p 794-808
10. M. Grujicic, J.R. Saylor, D.E. Beasley, W.S. DeRosset, and D. Helfritch, Computational Analysis of the Interfacial Bonding Between Feed-Powder Particles and the Substrate in the Cold-Gas Dynamic-Spray Process, *Appl. Surf. Sci.*, 2003, **219**(3-4), p 211-227
11. M. Grujicic, C.L. Zhao, C. Tong, W.S. DeRosset, and D. Helfritch, Analysis of the Impact Velocity of Powder Particles in the Cold-Gas Dynamic-Spray Process, *Mater. Sci. Eng. A*, 2004, **368**(1-2), p 222-230
12. T. Hussain, D.G. McCartney, P.H. Shipway, and D. Zhang, Bonding Mechanisms in Cold Spraying: The Contributions of Metallurgical and Mechanical Components, *J. Therm. Spray Technol.*, 2009, **18**(3), p 364-379
13. R.C.C. Dykhuizen, M.F.F. Smith, D.L.L. Gilmore, R.A.A. Neiser, X. Jiang, and S. Sampath, Impact of High Velocity Cold Spray Particles, *J. Therm. Spray Technol.*, 1999, **8**(4), p 559-564
14. T. Samson, D. MacDonald, R. Fernández, and B. Jodoin, Effect of Pulsed Waterjet Surface Preparation on the Adhesion Strength of Cold Gas Dynamic Sprayed Aluminum Coatings, *J. Therm. Spray Technol.*, 2015, **24**(6), p 984-993
15. H. Koivuluoto and P. Vuoristo, Structural Analysis of Cold-Sprayed Nickel-Based Metallic and Metallic–Ceramic Coatings, *J. Therm. Spray Technol.*, 2010, **19**(5), p 975-989
16. E. Irissou, J.G. Legoux, B. Arsenault, and C. Moreau, Investigation of Al-Al_2O_3 Cold Spray Coating Formation and Properties, *J. Therm. Spray Technol.*, 2007, **16**(5-6), p 661-668
17. A. Sova, A. Papyrin, and I. Smurov, Influence of Ceramic Powder Size on Process of Cermet Coating Formation by Cold Spray, *J. Therm. Spray Technol.*, 2009, **18**(4), p 633-641
18. Q. Wang, K. Spencer, N. Birbilis, and M.X. Zhang, The Influence of Ceramic Particles on Bond Strength of Cold Spray Composite Coatings on AZ91 Alloy Substrate, *Surf. Coat. Technol.*, 2010, **205**(1), p 50-56
19. A. Shkodkin, A. Kashirin, O. Klyuev, and T. Buzdygar, Metal Particle Deposition Stimulation by Surface Abrasive Treatment in Gas Dynamic Spraying, *J. Therm. Spray Technol.*, 2006, **15**(3), p 382-386
20. I. Finnie and D.H. McFadden, On the Velocity Dependence of the Erosion of Ductile Metals by Solid Particles at Low Angles of Incidence, *Wear*, 1978, **48**(1), p 181-190
21. A. Sova, V.F. Kosarev, A. Papyrin, and I. Smurov, Effect of Ceramic Particle Velocity on Cold Spray Deposition of Metal–Ceramic Coatings, *J. Therm. Spray Technol.*, 2011, **20**(1-2), p 285-291
22. Y.X. Wang, H. Yang, G. Lim, and Y. Li, Glass Formation Enhanced by Oxygen in Binary Zr-Cu System, *Scr. Mater.*, 2010, **62**(9), p 682-685
23. Y. Wang, B. Normand, N. Mary, M. Yu, and H. Liao, Effects of Ceramic Particle Size on Microstructure and the Corrosion Behavior of Cold Sprayed SiCp/Al 5056 Composite Coatings, *Surf. Coat. Technol.*, 2017, **315**, p 314-325
24. R.S. Lima, J. Karthikeyan, C.M. Kay, J. Lindemann, and C.C. Berndt, Microstructural Characteristics of Cold-Sprayed Nanostructured WC-Co Coatings, *Thin Solid Films*, 2002, **416**(1-2), p 129-135
25. F.S. da Silva, J. Bedoya, S. Dosta, N. Cinca, I.G. Cano, J.M. Guilemany, and A.V. Benedetti, Corrosion Characteristics of Cold Gas Spray Coatings of Reinforced Aluminum Deposited onto Carbon Steel, *Corros. Sci.*, 2017, **114**, p 57-71
26. E. Sansoucy, P. Marcoux, L. Ajdelsztajn, and B. Jodoin, Properties of SiC-Reinforced Aluminum Alloy Coatings Produced by the Cold Gas Dynamic Spraying Process, *Surf. Coat. Technol.*, 2008, **202**(16), p 3988-3996
27. W.Y. Li, G. Zhang, H.L. Liao, and C. Coddet, Characterizations of Cold Sprayed TiN Particle Reinforced Al2319 Composite Coating, *J. Mater. Process. Technol.*, 2008, **202**(1-3), p 508-513
28. S.V. Klinkov and V.F. Kosarev, Cold Spraying Activation Using an Abrasive Admixture, *J. Therm. Spray Technol.*, 2012, **21**(5), p 1046-1053
29. G.L. Eesley, A. Elmoursi, and N. Patel, Thermal Properties of Kinetic Spray Al-SiC Metal-Matrix Composite, *J. Mater. Res.*, 2003, **18**(4), p 855-860
30. K.S. Al-Hamdani, J.W. Murray, T. Hussain, A. Kennedy, and A.T. Clare, Cold Sprayed Metal–Ceramic Coatings Using Satellited Powders, *Mater. Lett.*, 2017, **198**, p 184-187
31. B. Aldwell, S. Yin, K.A. McDonnell, D. Trimble, T. Hussain, and R. Lupoi, A Novel Method for Metal–Diamond Composite Coating Deposition with Cold Spray and Formation Mechanism, *Scr. Mater.*, 2016, **115**, p 10-13
32. Y.T.R. Lee, H. Ashrafizadeh, G. Fisher, and A. McDonald, Effect of Type of Reinforcing Particles on the Deposition Efficiency and Wear Resistance of Low-Pressure Cold-Sprayed Metal Matrix Composite Coatings, *Surf. Coat. Technol.*, 2017, **324**, p 190-200
33. P.E. Leger, M. Sennour, F. Delloro, F. Borit, A. Debray, F. Gaslain, M. Jeandin, and M. Ducos, Multiscale Experimental and Numerical Approach to the Powder Particle Shape Effect on Al-Al2O3 Coating Build-Up, *J. Therm. Spray Technol.*, 2017, **26**(7), p 1445-1460
34. M. Yu, W.-Y.Y. Li, X.K.K. Suo, and H.L.L. Liao, Effects of Gas Temperature and Ceramic Particle Content on Microstructure and Microhardness of Cold Sprayed SiCp/Al 5056 Composite Coatings, *Surf. Coat. Technol.*, 2013, **220**, p 102-106
35. M. Yu, X.K.K. Suo, W.Y.Y. Li, Y.Y.Y. Wang, and H.L.L. Liao, Microstructure, Mechanical Property and Wear Performance of Cold Sprayed Al5056/SiCp Composite Coatings: Effect of Reinforcement Content, *Appl. Surf. Sci.*, 2014, **289**, p 188-196
36. C.J. Huang and W.Y. Li, Strengthening Mechanism and Metal/Ceramic Bonding Interface of Cold Sprayed TiN $_p$/Al5356 Deposits, *Surf. Eng.*, 2016, **32**(9), p 663-669
37. K. Spencer, D.M. Fabijanic, and M.X. Zhang, The Use of Al-Al2O3 Cold Spray Coatings to Improve the Surface Properties of Magnesium Alloys, *Surf. Coat. Technol.*, 2009, **204**(3), p 336-344

38. H.Y. Lee, Y.H. Yu, Y.C. Lee, Y.P. Hong, and K.H. Ko, Cold Spray of SiC and Al_2O_3 with Soft Metal Incorporation: A Technical Contribution, *J. Therm. Spray Technol.*, 2004, **13**(2), p 184-189
39. C. Feng, V. Guipont, M. Jeandin, O. Amsellem, F. Pauchet, R. Saenger, S. Bucher, and C. Iacob, B4C/Ni Composite Coatings Prepared by Cold Spray of Blended or CVD-Coated Powders, *J. Therm. Spray Technol.*, 2012, **21**(3-4), p 561-570
40. J.M. Shockley, S. Descartes, P. Vo, E. Irissou, and R.R. Chromik, The Influence of Al_2O_3 Particle Morphology on the Coating Formation and Dry Sliding Wear Behavior of Cold Sprayed Al-Al_2O_3 Composites, *Surf. Coatings Technol.*, 2015, **270**, p 324-333
41. R.G. Maev and E. Leshchinsky, "Low Pressure Gas Dynamic Spray: Shear Localization during Particle Shock Consolidation," *Thermal Spray 2006: Science, Innovation and Application*, 2006.
42. R.G. Maev and V. Leshchynsky, Air Gas Dynamic Spraying of Powder Mixtures: Theory and Application, *J. Therm. Spray Technol.*, 2006, **15**(2), p 198-205
43. I. Finnie, Erosion of Surfaces by Solid Particles, *Wear*, 1960, **3**(2), p 87-103
44. J.H. Neilson and A. Gilchrist, Erosion by a Stream of Solid Particles, *Wear*, 1968, **11**(2), p 111-122
45. Y. Xie, M.P. Planche, R. Raoelison, P. Hervé, X. Suo, P. He, and H. Liao, Investigation on the Influence of Particle Preheating Temperature on Bonding of Cold-Sprayed Nickel Coatings, *Surf. Coat. Technol.*, 2017, **318**, p 99-105
46. F. Gärtner, C. Borchers, T. Stoltenhoff, H. Kreye, and H. Assadi, Numerical and Microstructural Investigations of the Bonding Mechanisms in Cold Spraying, *Thermal Spray 2003: Advancing the Science and Applying the Technology*, B.R. Marple and C. Moreau, Ed., May 5–8, 2003 (Orlando, FL), ASM International, 2003, vol 1, p 845, vol 2, p 864.
47. M. Grujicic, C.L. Zhao, W.S. DeRosset, and D. Helfritch, Adiabatic Shear Instability Based Mechanism for Particles/substrate Bonding in the Cold-Gas Dynamic-Spray Process, *Mater. Des.*, 2004, **25**(8), p 681-688
48. J.G.A. Bitter, A Study of Erosion Phenomena, *Wear*, 1963, **6**(3), p 169-190
49. X. Wang, F. Feng, M.A. Klecka, M.D. Mordasky, J.K. Garofano, T. El-Wardany, A. Nardi, and V.K. Champagne, Characterization and Modeling of the Bonding Process in Cold Spray Additive Manufacturing, *Addit. Manuf.*, 2015, **8**, p 149-162
50. G. Bae, Y. Xiong, S. Kumar, K. Kang, and C. Lee, General Aspects of Interface Bonding in Kinetic Sprayed Coatings, *Acta Mater.*, 2008, **56**(17), p 4858-4868
51. F. Meng, H. Aydin, S. Yue, and J. Song, The Effects of Contact Conditions on the Onset of Shear Instability in Cold-Spray, *J. Therm. Spray Technol.*, 2015, **24**(4), p 711-719
52. X. Bin Wang, Adiabatic Shear Localization for Steels Based on Johnson–Cook Model and Second- and Fourth-Order Gradient Plasticity Models, *J. Iron Steel Res. Int.*, 2007, **14**(5), p 56-61
53. Z.S. Liu, S. Swaddiwudhipong, and M.J. Islam, Perforation of Steel and Aluminum Targets Using a Modified Johnson-Cook Material Model, *Nucl. Eng. Des.*, 2012, **250**, p 108-115
54. Y. Cormier, P. Dupuis, B. Jodoin, and A. Ghaei, Finite Element Analysis and Failure Mode Characterization of Pyramidal Fin Arrays Produced by Masked Cold Gas Dynamic Spray, *J. Therm. Spray Technol.*, 2015, **24**(8), p 1549-1565
55. P.C. King, G. Bae, S.H. Zahiri, M. Jahedi, and C. Lee, An Experimental and Finite Element Study of Cold Spray Copper Impact onto Two Aluminum Substrates, *J. Therm. Spray Technol.*, 2010, **19**(3), p 620-634
56. M. Saleh, V. Luzin, and K. Spencer, Analysis of the Residual Stress and Bonding Mechanism in the Cold Spray Technique Using Experimental and Numerical Methods, *Surf. Coat. Technol.*, 2014, **252**, p 15-28
57. A. Papyrin, *Cold Spray Technology. Advanced Materials and Processing*, Elsevier, Amsterdam, 2001
58. J.G. Legoux, E. Irissou, and C. Moreau, Effect of Substrate Temperature on the Formation Mechanism of Cold-Sprayed Aluminum, Zinc and Tin Coatings, *J. Therm. Spray Technol.*, 2007, **16**(5-6), p 619-626
59. K.J. Hodder, J.A. Nychka, and A.G. McDonald, Comparison of 10 Mm and 20 Nm Al-Al_2O_3 Metal Matrix Composite Coatings Fabricated by Low-Pressure Cold Gas Dynamic Spraying, *J. Therm. Spray Technol.*, 2014, **23**(5), p 839-848
60. J. Wu, H. Fang, S. Yoon, H. Kim, and C. Lee, Measurement of Particle Velocity and Characterization of Deposition in Aluminum Alloy Kinetic Spraying Process, *Appl. Surf. Sci.*, 2005, **252**(5), p 1368-1377
61. K.J. Hodder, H. Izadi, A.G. McDonald, and A.P. Gerlich, Fabrication of Aluminum–Alumina Metal Matrix Composites via Cold Gas Dynamic Spraying at Low Pressure Followed by Friction Stir Processing, *Mater. Sci. Eng. A*, 2012, **556**, p 114-121
62. N.M. Melendez, V.V. Narulkar, G.A. Fisher, and A.G. McDonald, Effect of Reinforcing Particles on the Wear Rate of Low-Pressure Cold-Sprayed WC-Based MMC Coatings, *Wear*, 2013, **306**(1-2), p 185-195
63. S.A. Alidokht, P. Manimunda, P. Vo, S. Yue, and R.R. Chromik, Cold Spray Deposition of a Ni-WC Composite Coating and Its Dry Sliding Wear Behavior, *Surf. Coat. Technol.*, 2016, **308**, p 424-434